

***R*-matrix electron-impact excitation data for the Ne-like iso-electronic sequence[★]**

G. Y. Liang and N. R. Badnell

Department of Physics, University of Strathclyde, Glasgow, G4 0NG, UK
e-mail: guiyun.liang@strath.ac.uk

Received 1 February 2010 / Accepted 7 May 2010

ABSTRACT

We present results for the electron-impact excitation of all Ne-like ions from Na⁺ to Kr²⁶⁺ obtained using the intermediate-coupling frame transformation *R*-matrix approach. For each ion's calculation, the close-coupling expansion is taken to be the 113 LS terms (209 levels) belonging to the configurations [1s²]2s²2p⁶, 2s²2p⁵{3, 4, 5}*l*, 2s2p⁶{3, 4, 5}*l* (*l* ∈ s, p, d, f, and g), and 2s²2p⁵{6, 7}*l*' (*l*' ∈ s, p, and d). An additional configuration interaction effect arising from configurations of 2s²2p⁴3*l*{3, 4, 5}*l*'' (*l*'' ∈ s, p, d, f and g) was included in the target expansion. A detailed comparison of the target structure has been made for six specific ions (Si⁴⁺, Ar⁸⁺, Ca¹⁰⁺, Fe¹⁶⁺, Ni¹⁸⁺, and Kr²⁶⁺) spanning the sequence to assess the accuracy for the entire sequence. Effective collision strengths (Υs) are presented at temperatures ranging from 2 × 10²(*q*+1)² K to 2 × 10⁶(*q*+1)² K (where *q* is the residual charge of ions, i.e. *Z* − 10). Detailed comparisons for the Υs are made with the results of previous calculations for several ions, which span the sequence. Furthermore, we examine the iso-electronic trends of effective collision strengths as a function of temperature. The present results are the only *R*-matrix ones for the majority of the ions and the most extensive and complete data for modelling to-date.

Key words. atomic data – atomic processes – plasmas

1. Introduction

Because Ne-like ions have a stable closed L-shell ground state, they show high abundance over a wide range of temperatures in ionization equilibrium for each iso-nuclear sequence (see Mazzotta et al. 1998; Bryans et al. 2006, 2009). Thus, they attract extensive studies for spectral diagnostic and modelling in astrophysical and laboratory plasmas, and in particular iron, due to its high cosmic abundance. X-ray lasers (Mathews et al. 1985; Tomasel et al. 1997) based on Ne-like ions are another significant area of interest. However, the atomic structure and electron-impact excitation (EIE) of Ne-like ions are extremely complex, which results in there being large uncertainties in line intensity ratios (2p⁵3d ¹P₁ → 2p⁶ ¹S₀ vs 2p⁵3d ³D₁ → 2p⁶ ¹S₀, this is usually designated 3C/3D, as well as 3s − 2p vs. 3C) between measurements or observations and predictions (Beiersdorfer et al. 2001, 2002; Gu et al. 2004). For example, even for iron, EIE of this ion has been investigated experimentally and theoretically for a long time (Smith et al. 1985; Chen et al. 2003; Loch et al. 2006; Beiersdorfer et al. 2001, 2002 and references therein).

Resonances in electron-ion impact excitation have been observed in laboratory measurements (Brown et al. 2006). They play an important role in the spectral diagnostic and modelling of astrophysical and laboratory plasmas. The close-coupling (CC) approximation (e.g. *R*-matrix, Hummer et al. 1993) satisfactorily

reproduces and describes such resonances. Recently, there have been several works using this method for three ions in this iso-electronic sequence. Chen et al. (2003) performed (BPRM) Breit-Pauli *R*-matrix (Berrington et al. 1995) calculations for Fe¹⁶⁺ with an 89 fine-structure level close-coupling expansion (to *n* = 4). Loch et al. (2006) performed a fully-relativistic larger scale Fe¹⁶⁺ calculation (139 fine-structure levels, including an additional 50 levels of the 2p⁵5*l* configurations) using the Dirac atomic *R*-matrix code (DARC, Norrington & Grant 1987). Collisional-radiative (CR) modelling with their updated excitation data was also undertaken (Chen 2008; Loch et al. 2006), the combination of which gives satisfactory agreement between measurements/observations and theory for the 3C/3D line ratio. A benchmark work performed by Del Zanna & Ishikawa (2009) revealed the data of Loch et al. (2006) to be reliable. Similar differences for other (non-iron) ions in this iso-electronic sequence have been observed between measurements (Beiersdorfer et al. 2001) and theoretical predictions based upon distorted-wave (DW) excitation data. By making a semi-empirical configuration-interaction (CI) correction to excitation data and taking CR effects into account, Fournier & Hansen (2005) brought the predictions into agreement with measurements for Ne-like ions from Cr¹⁴⁺ to Ag³⁷⁺. This confirms again that accurate atomic data is essential for the reliable diagnostic modelling of astrophysical and laboratory plasmas. However, most excitation data in this iso-electronic sequence are from the DW approximation (Zhang et al. 1987; Bhatia et al. 1985), except for *R*-matrix calculations for three ions, viz Fe¹⁶⁺ (BPRM and DARC, as noted above), Ni¹⁸⁺, and Kr²⁶⁺ (both DARC). For Ni¹⁸⁺, Aggarwal & Keenan (2008) performed an 89-level CC

[★] These data are made available in the archives of APAP via <http://www.apap-network.org>, OPEN-ADAS via <http://open.adas.ac.uk> as well as anonymous ftp to [cdsarc.u-strasbg.fr](ftp://cdsarc.u-strasbg.fr) (130.79.128.5) or via <http://cdsweb.u-strasbg.fr/cgi-bin/qcat?J/A+A/518/A64>

($n = 4$, $[1s^2]2s^22p^6$, $2s^22p^5\{3, 4\}l$, and $2s2p^6\{3, 4\}l$) calculation and Chen et al. (2006) a 125-level ($[1s^2]2s^22p^6$, $2s^22p^5\{3, 4, 5\}l$, and $2s2p^6\{3, 4\}l$) CC calculation. For Kr^{26+} , Griffin et al. (2008) used a 139-level ($n = 5$, $[1s^2]2s^22p^6$, $2s^22p^5\{3, 4, 5\}l$, $2s2p^6\{3, 4\}l$) CC expansion; they also demonstrated that the radiative damping of resonance contributions is a small effect.

Due to the advantage of high accuracy – see Griffin et al. (1998), Badnell & Griffin (1999), Berrington et al. (2005) and Liang et al. (2008) – and computational efficiency of the intermediate-coupling frame transformation (ICFT) R -matrix methodology and associated codes, along with the high capability of parallel computer clusters, it is now feasible to provide excitation data for iso-electronic sequences across the entire range of astrophysical interest within the R -matrix framework. Witthoef et al. (2007) investigated the physics of electron-impact excitation along the F-like iso-electronic sequence (Ne^+ to Kr^{27+}) and Liang et al. (2009a,b) also did an entire sequence calculation for Na-like ions (for both outer- and inner-shell excitations) with Auger- and radiative-damping included for the inner-shell excitations. Based upon the robustness of the current suite of R -matrix codes, the R -matrix calculation of effective collision strengths (Υ) currently can be performed automatically for each ion without manual intervention along an iso-electronic sequence after sufficiently accurate radial wave functions have been obtained and CI/CC expansions have been confirmed. This ensures that each calculation is performed uniformly and reliably, as well as that the calculation along the sequence is consistent. Careful analysis of the results for several specified ions spanning the sequence is still necessary so as to further validate the accuracy of the data along the sequence.

In this paper, we report on the electron-impact excitation of the Ne-like iso-electronic sequence (from Na^+ to Kr^{26+}), via the ICFT R -matrix approach. In Sect. 2, we discuss details of the calculation method and pay particular attention on comparing our underlying atomic structure with previous results. The excitation results themselves are discussed in Sect. 3. Our work is a part of ongoing collaborative work – the UK Atomic Processes for Astrophysical Plasmas (APAP) network¹, a broadening of scope of the original UK RmaX network.

2. Sequence calculation

The aim of this work is to perform R -matrix calculations employing the ICFT method (see Griffin et al. 1998) for all Ne-like ions from Na^+ to Kr^{26+} . In our calculations we included the following 31 configuration basis set in our close-coupling expansion: $[1s^2]2s^22p^6$, $2s^22p^5\{3, 4, 5\}l$, $2s2p^6\{3, 4, 5\}l$ ($l \in s, p, d, f$ and g) and $2s^22p^5\{6, 7\}l'$ ($l' \in s, p$ and d), and an additional 33 correlation configuration – $2s^22p^43l\{3, 4, 5\}l'$ (l and $l' \in s, p, d, f$ and g) in our CI expansion. This results in 113 close-coupling LS terms and 209 fine-structure levels. The CI expansion consists of 1337 LS terms and 2775 fine-structure levels, which were determined to be important for improving the accuracy of the energy levels which we included in the close-coupling expansion.

2.1. Structure: energies

The target wave functions (1s-7d) were obtained from AUTOSTRUCTURE (AS, Badnell 1986) using the Thomas-Fermi-Dirac-Amaldi model potential. Relativistic effects were included perturbatively via the one-body Breit-Pauli operator (viz. mass-velocity, spin-orbit and Darwin) without valence electron

Table 1. Radial scaling factors used in AUTOSTRUCTURE to minimize the total energies of $2s^22p^6$ ($2s$ and $2p$ orbitals) and $2s^22p^53l$ ($3l$ orbitals) complexes, respectively – see text for details.

| Ion | 2s | 2p | 3s | 3p | 3d |
|-----|---------|---------|---------|---------|---------|
| Na | 1.05325 | 0.99028 | 1.00144 | 1.10304 | 0.89098 |
| Mg | 1.06060 | 0.99638 | 1.02899 | 1.07656 | 0.93850 |
| Al | 1.06828 | 1.00060 | 1.04887 | 1.06575 | 0.96022 |
| Si | 1.07620 | 1.00403 | 1.06486 | 1.06016 | 0.97781 |
| P | 1.08461 | 1.00718 | 1.07860 | 1.05719 | 0.99100 |
| S | 1.09407 | 1.01029 | 1.09126 | 1.05619 | 1.00123 |
| Cl | 1.10436 | 1.01354 | 1.10346 | 1.05599 | 1.00949 |
| Ar | 1.11591 | 1.01700 | 1.11559 | 1.05671 | 1.01639 |
| K | 1.12858 | 1.02117 | 1.12792 | 1.05767 | 1.02320 |
| Ca | 1.14291 | 1.02568 | 1.14068 | 1.05846 | 1.02863 |
| Sc | 1.15928 | 1.03048 | 1.15407 | 1.06061 | 1.03362 |
| Ti | 1.17769 | 1.03588 | 1.16830 | 1.06364 | 1.03784 |
| V | 1.19835 | 1.04209 | 1.18353 | 1.06712 | 1.04196 |
| Cr | 1.22166 | 1.04889 | 1.19942 | 1.07165 | 1.04607 |
| Mn | 1.24853 | 1.05616 | 1.21647 | 1.07698 | 1.05021 |
| Fe | 1.27826 | 1.06471 | 1.23503 | 1.08299 | 1.05443 |
| Co | 1.31154 | 1.07401 | 1.25541 | 1.09006 | 1.05875 |
| Ni | 1.35010 | 1.08401 | 1.27760 | 1.09825 | 1.06316 |
| Cu | 1.39467 | 1.09579 | 1.30170 | 1.10729 | 1.06765 |
| Zn | 1.44425 | 1.10831 | 1.32832 | 1.11769 | 1.07230 |
| Ga | 1.50306 | 1.12207 | 1.35715 | 1.12929 | 1.07705 |
| Ge | 1.56998 | 1.13722 | 1.38861 | 1.14226 | 1.08194 |
| As | 1.64873 | 1.15409 | 1.42305 | 1.15656 | 1.08695 |
| Se | 1.74083 | 1.17262 | 1.46051 | 1.17235 | 1.09212 |
| Br | 1.85007 | 1.19293 | 1.50166 | 1.18969 | 1.09746 |
| Kr | 1.98387 | 1.21520 | 1.54677 | 1.20864 | 1.10295 |

two-body fine-structure operators. This is consistent with the operators included in the standard Breit-Pauli R -matrix suite of codes. The radial scaling parameters, λ_{nl} ($n = 2$ and 3 ; $l \in s, p$ and d), were obtained separately for each ion by a two-step optimization procedure with $\lambda_{\{1,4,5,6,7\}l} = 1.00$. In the first step, the energy of the ground level $2s^22p^6\ ^1S_0$ was minimized by varying the λ_{2s} and λ_{2p} scaling parameters. Then, the average-energy of the fine-structure levels of the 14 terms of the $2s^22p^53l$ configuration was minimized by varying the λ_{3l} scaling parameters. This optimization procedure was found to be the best common one that could be used for all ions over the sequence. Optimizing the nl ($n = 4, 5, 6$ and 7) orbitals was found to give only a small improvement of the target level energies for several specified ions (Si^{4+} , Fe^{16+} and Kr^{26+}) spanning the sequence. In order to maintain consistency and so as not to introduce arbitrary changes along the sequence, the optimization procedure is done automatically in AUTOSTRUCTURE without any manual re-adjustment. The resultant scaling parameters are listed in Table 1.

A comparison of level energies with previous calculations and data, derived semi-empirically from experimental energies, available from the compilation of NIST v3² or observed values available in the CHIANTI v6 database and astrophysical modelling code (Dere et al. 2009) was made for several specific ions (Si^{4+} , Ar^{8+} , Ca^{10+} , Fe^{16+} , Ni^{18+} and Kr^{26+}) spanning the sequence so as to assess the accuracy of our present AS calculations over the entire iso-electronic series. Tables 2, 4, 6, 8, 10, and 12 list various theoretical level energies along with NIST

¹ <http://www.apap-network.org>

² <http://physics.nist.gov/PhysRefData/ASD/index.html>

Table 2. The level energies (Ryd) of Si⁴⁺ from different calculations along with the compilation of NIST v3².

| ID | Level specification | NIST ^a | AS | FAC | CHIANTI ^b | MCHF ^c |
|----|--|-------------------|-----------|-----------|----------------------|-------------------|
| 1 | 2s ² 2p ⁶ 1S ₀ | | 0.000000 | 0.000000 | 0.000000 | |
| 2 | 2s ² 2p ⁵ 3s 3P ₂ | 7.636576 | 7.627520 | 7.645096 | 7.471944 | 7.636311 |
| 3 | 2s ² 2p ⁵ 3s 3P ₁ | 7.660020 | 7.651149 | 7.669024 | 7.496347 | 7.659752 |
| 4 | 2s ² 2p ⁵ 3s 3P ₀ | 7.682625 | 7.672594 | 7.689856 | 7.518236 | 7.682296 |
| 5 | 2s ² 2p ⁵ 3s 1P ₁ | 7.732203 | 7.727683 | 7.750462 | 7.576521 | 7.731955 |
| 6 | 2s ² 2p ⁵ 3p 3S ₁ | 8.258379 | 8.246423 | 8.256845 | 8.101019 | 8.258102 |
| 7 | 2s ² 2p ⁵ 3p 3D ₃ | 8.364780 | 8.359913 | 8.372963 | 8.189849 | 8.364501 |
| 8 | 2s ² 2p ⁵ 3p 3D ₂ | 8.374174 | 8.369346 | 8.384104 | 8.198962 | 8.373860 |
| 9 | 2s ² 2p ⁵ 3p 3D ₁ | 8.391529 | 8.386711 | 8.399595 | 8.215911 | 8.391069 |
| 10 | 2s ² 2p ⁵ 3p 1D ₂ | 8.422766 | 8.418290 | 8.434033 | 8.250539 | 8.422583 |
| 11 | 2s ² 2p ⁵ 3p 1P ₁ | 8.437853 | 8.436352 | 8.450207 | 8.264883 | 8.437552 |
| 12 | 2s ² 2p ⁵ 3p 3P ₂ | 8.451074 | 8.446452 | 8.462297 | 8.278670 | 8.450769 |
| 13 | 2s ² 2p ⁵ 3p 3P ₀ | 8.454788 | 8.451684 | 8.464687 | 8.280566 | 8.454470 |
| 14 | 2s ² 2p ⁵ 3p 3P ₁ | 8.460253 | 8.457485 | 8.472367 | 8.286872 | 8.459926 |
| 15 | 2s ² 2p ⁵ 3p 1S ₀ | 8.77505 | 8.876968 | 8.922108 | 8.851711 | 8.774769 |
| 16 | 2s ² 2p ⁵ 3d 3P ₀ | 9.273318 | 9.270566 | 9.267329 | 9.103458 | 9.273033 |
| 17 | 2s ² 2p ⁵ 3d 3P ₁ | 9.278845 | 9.276363 | 9.272374 | 9.109172 | 9.278537 |
| 18 | 2s ² 2p ⁵ 3d 3P ₂ | 9.290708 | 9.288542 | 9.284232 | 9.121027 | 9.290319 |
| 19 | 2s ² 2p ⁵ 3d 3F ₄ | 9.307536 | 9.309413 | 9.305353 | 9.132764 | 9.307223 |
| 20 | 2s ² 2p ⁵ 3d 3F ₃ | 9.316348 | 9.318389 | 9.316576 | 9.142041 | 9.316025 |
| 21 | 2s ² 2p ⁵ 3d 3F ₂ | 9.333562 | 9.335089 | 9.332421 | 9.158398 | 9.333074 |
| 22 | 2s ² 2p ⁵ 3d 1F ₃ | 9.345281 | 9.349206 | 9.347836 | 9.172796 | 9.345075 |
| 23 | 2s ² 2p ⁵ 3d 1D ₂ | 9.380647 | 9.383311 | 9.381456 | 9.205793 | 9.379566 |
| 24 | 2s ² 2p ⁵ 3d 3D ₁ | 9.380036 | 9.384037 | 9.383614 | 9.206276 | 9.380304 |
| 25 | 2s ² 2p ⁵ 3d 3D ₃ | 9.384912 | 9.387550 | 9.386841 | 9.210350 | 9.384568 |
| 26 | 2s ² 2p ⁵ 3d 3D ₂ | 9.389823 | 9.392712 | 9.392014 | 9.215362 | 9.389434 |
| 27 | 2s ² 2p ⁵ 3d 1P ₁ | 9.449065 | 9.463153 | 9.471244 | 9.302779 | 9.448883 |
| 28 | 2s ² 2p ⁵ 4s 3P ₂ | 10.01823 | 10.025722 | 10.021532 | | 10.017768 |
| 29 | 2s ² 2p ⁵ 4s 3P ₁ | 10.03067 | 10.038223 | 10.036309 | | 10.030362 |
| 30 | 2s ² 2p ⁵ 4s 3P ₀ | 10.06444 | 10.070616 | 10.066578 | | 10.063904 |
| 31 | 2s ² 2p ⁵ 4s 1P ₁ | 10.07483 | 10.081318 | 10.081030 | | 10.074475 |
| 32 | 2s ² 2p ⁵ 4p 3S ₁ | 10.24486 | 10.248513 | 10.246311 | | |
| 33 | 2s ² 2p ⁵ 4p 3D ₃ | 10.27825 | 10.282198 | 10.285662 | | |
| 34 | 2s ² 2p ⁵ 4p 3D ₂ | 10.28347 | 10.287772 | 10.292513 | | |
| 35 | 2s ² 2p ⁵ 4p 1P ₁ | 10.29257 | 10.297196 | 10.302666 | | |
| 36 | 2s ² 2p ⁵ 4p 3P ₂ | 10.29820 | 10.302854 | 10.309430 | | |
| 37 | 2s ² 2p ⁵ 4p 3P ₀ | 10.32510 | 10.330410 | 10.337097 | | |
| 38 | 2s ² 2p ⁵ 4p 3D ₁ | 10.32766 | 10.331017 | 10.335484 | | |
| 39 | 2s ² 2p ⁵ 4p 1D ₂ | 10.33545 | 10.338814 | 10.345399 | | |
| 40 | 2s ² 2p ⁵ 4p 3P ₁ | 10.33545 | 10.339068 | 10.344921 | | |
| 41 | 2s ² 2p ⁵ 4p 1S ₀ | 10.43362 | 10.491684 | 10.528749 | | |
| 42 | 2s ² 2p ⁵ 4d 3P ₀ | 10.59995 | 10.606728 | 10.600389 | | |
| 43 | 2s ² 2p ⁵ 4d 3P ₁ | 10.60383 | 10.610847 | 10.604652 | | |
| 44 | 2s ² 2p ⁵ 4d 3P ₂ | 10.61133 | 10.618787 | 10.613007 | | |
| 45 | 2s ² 2p ⁵ 4d 3F ₄ | 10.61303 | 10.621538 | 10.616589 | | |
| 46 | 2s ² 2p ⁵ 4d 3F ₃ | 10.61793 | 10.626940 | 10.623125 | | |
| 47 | 2s ² 2p ⁵ 4d 1D ₂ | 10.62689 | 10.636085 | 10.632943 | | |
| 48 | 2s ² 2p ⁵ 4d 3D ₃ | 10.63038 | 10.640347 | 10.638092 | | |
| 49 | 2s ² 2p ⁵ 4d 3D ₁ | 10.64926 | 10.661087 | 10.660041 | | |
| 50 | 2s ² 2p ⁵ 4d 3F ₂ | 10.66570 | 10.673565 | 10.670477 | | |
| 51 | 2s ² 2p ⁵ 4d 3D ₂ | 10.66860 | 10.676813 | 10.674084 | | |
| 52 | 2s ² 2p ⁵ 4d 1F ₃ | 10.66937 | 10.677815 | 10.675137 | | |
| 53 | 2s ² 2p ⁵ 4f 3D ₁ | 10.68445 | 10.689679 | 10.689431 | | |
| 54 | 2s ² 2p ⁵ 4f 3D ₂ | 10.68502 | 10.690324 | 10.690251 | | |
| 55 | 2s ² 2p ⁵ 4f 3G ₅ | 10.68812 | 10.694274 | 10.694413 | | |
| 56 | 2s ² 2p ⁵ 4f 1G ₄ | 10.68821 | 10.694326 | 10.694619 | | |
| 57 | 2s ² 2p ⁵ 4f 3D ₃ | 10.69027 | 10.695958 | 10.696143 | | |
| 58 | 2s ² 2p ⁵ 4f 1D ₂ | 10.69082 | 10.696471 | 10.697012 | | |
| 59 | 2s ² 2p ⁵ 4f 1F ₃ | 10.69390 | 10.700062 | 10.700759 | | |
| 60 | 2s ² 2p ⁵ 4f 3F ₄ | 10.69399 | 10.700209 | 10.700871 | | |

Notes. ^(a) Sources of NIST v3 are from the work of [Martin & Zalubas \(1983\)](#) and references therein. ^(b) Theoretical energies from [Bhatia et al. \(1985\)](#). ^(c) Data is calculated with multiconfiguration Hartree-Fock (MCHF) or multiconfiguration Dirac-Fock (MCDF) method, and available from website: <http://atoms.vuse.vanderbilt.edu/>

(v3) derived or CHIANTI (v6) observed ones for the 60 lowest-lying levels. A fully relativistic calculation with the Flexible Atomic Code (FAC, Gu 2008) was also performed for these ions with only CI from $2s^2 2p^4 3/3/1'$ included besides that of the CC configurations. This is because a correction of level energies has been carried-out by using the difference of average configuration energy obtained using a different orbital basis for each configuration and that obtained using the unique orbital basis required for multiconfiguration level structure – see Gu (2008) and the FAC manual for details. Such a procedure is not readily usable in an R -matrix calculation. A complete comparison with available NIST experimentally derived or CHIANTI observed data is shown in Fig. 1. A complete set of level energies from the present AS calculation is available electronically³. Figure 1 and Tables 2, 4, 6, 8, 10, and 12 show that excellent agreement (within 0.5%) is obtained when compared with NIST derived or CHIANTI observed data except for a few energy levels. Moreover, better agreement (0.3%) is obtained for Si^{4+} , Ar^{8+} , Fe^{16+} , Ni^{18+} , etc.

For Si^{4+} , the results of Bhatia et al. (1985) currently used by the CHIANTI are lower than the NIST data by 1.5%–2.3%. The results from multiconfiguration Hartree-Fock (MCHF) or multiconfiguration Dirac-Fock (MCDF) method available from the MCHF/MCDF Collection⁴ show excellent agreement with the NIST data. For Ar^{8+} , Ca^{10+} and Ni^{18+} , the calculation of Zhang et al. (1987) was adopted by CHIANTI, showing the same level of accuracy with the present AS calculation. For Fe^{16+} , the present AS data is systematically higher than that of Landi & Gu (2006) used by CHIANTI by $\sim 0.4\%$. However, both show a better level of accuracy (0.2%) when compared with NIST data. Calculations with the MCDF method have been done for highly charged ions, e.g. Fe^{16+} (Aggarwal et al. 2003), Ni^{18+} (Aggarwal & Keenan 2006) and Kr^{26+} (Griffin et al. 2008) recently. When compared with them, the present AS data agrees also to within 0.4%. This means that our atomic structure is accurate, and the target expansion of 31 spectroscopic configurations and additional 33 correlation configurations in scattering calculation is reliable along the Ne-like iso-electronic sequence.

2.2. Structure: weighted oscillator strength

A further test of our structure calculations is to compare weighted oscillator strengths ($g_i f_{i,j}$ for a given $i \leftarrow j$ transition, where g_i is statistical weight of the initial level i and f is the oscillator strength of the transition) with those of other calculations. Tables 3, 5, 7, 9, 11, and 13 show a detailed comparison for a selection of gf -values from the 5 lowest-lying levels for six ions spanning the sequence: Si^{4+} , Ar^{8+} , Ca^{10+} , Fe^{16+} , Ni^{18+} and Kr^{26+} .

For Si^{4+} , around 68% of transitions available⁵ from the CHIANTI v6 database (Dere et al. 2009) show agreement to within 20% between the present AS calculations and the results of Bhatia et al. (1985). There are about 56% of all-type transitions (this refers to dipole and quadrupole) showing $|1.0 - gf_v/gf_L| \leq 20\%$ with $gf_L \geq 0.001$ (gf_v and gf_L are weighted oscillator strengths in velocity and length gauges, respectively). As shown in Table 3, the present AS calculation also shows good agreement with the results of our FAC calculations and the MCHF ones⁴.

Table 3. Comparison of the weighted oscillator strength gf between the AS and other calculations for Si^{4+} .

| $i - j$ | AS | | CHIANTI ^a | FAC | MCHF ^b |
|---------|--------------|-------------|----------------------|-------------|-------------------|
| | gf_L | gf_v/gf_L | | | |
| 1–3 | 2.19^{-2c} | 0.89 | 2.36^{-2} | 2.09^{-2} | 2.44^{-2} |
| 1–5 | 2.33^{-1} | 0.92 | 2.82^{-1} | 2.68^{-1} | 2.18^{-1} |
| 1–17 | 2.63^{-3} | 0.94 | 2.62^{-3} | 2.56^{-3} | 2.98^{-3} |
| 1–24 | 7.97^{-2} | 0.95 | 6.54^{-2} | 6.23^{-2} | 1.03^{-1} |
| 1–27 | 1.17^{+0} | 0.96 | 1.46^{+0} | 1.25^{+0} | 1.02^{+0} |
| 2–6 | 3.58^{-1} | 0.86 | 4.25^{-1} | 3.49^{-1} | 3.55^{-1} |
| 2–7 | 1.59^{+0} | 0.97 | 1.54^{+0} | 1.58^{+0} | 1.55^{+0} |
| 2–8 | 4.24^{-1} | 0.93 | 4.28^{-1} | 4.27^{-1} | 4.21^{-1} |
| 2–9 | 6.08^{-2} | 0.89 | 5.80^{-2} | 5.89^{-2} | 6.13^{-2} |
| 2–10 | 5.00^{-1} | 0.81 | 4.89^{-1} | 5.20^{-1} | 5.16^{-1} |
| 2–11 | 6.09^{-2} | 0.78 | 5.10^{-2} | 5.94^{-2} | 4.34^{-2} |
| 2–12 | 2.91^{-1} | 0.75 | 2.00^{-1} | 2.63^{-1} | 2.45^{-1} |
| 2–14 | 1.49^{-1} | 0.79 | 1.27^{-1} | 1.55^{-1} | 1.55^{-1} |
| 3–6 | 1.42^{-1} | 0.87 | 1.63^{-1} | 1.43^{-1} | 1.37^{-1} |
| 3–8 | 6.92^{-1} | 0.99 | 6.52^{-1} | 6.83^{-1} | 6.71^{-1} |
| 3–9 | 4.06^{-1} | 0.94 | 3.92^{-1} | 3.91^{-1} | 4.05^{-1} |
| 3–10 | 1.88^{-1} | 0.84 | 2.34^{-1} | 2.08^{-1} | 2.27^{-1} |
| 3–11 | 5.58^{-2} | 0.79 | 4.27^{-2} | 5.59^{-2} | 4.59^{-2} |
| 3–12 | 2.78^{-1} | 0.82 | 2.18^{-1} | 2.61^{-1} | 2.30^{-1} |
| 3–13 | 2.34^{-1} | 0.80 | 2.17^{-1} | 2.36^{-1} | 2.27^{-1} |
| 3–14 | 4.86^{-2} | 0.72 | 5.34^{-2} | 5.59^{-2} | 5.05^{-2} |
| 3–15 | 2.77^{-2} | 0.66 | 4.09^{-2} | 2.42^{-2} | 2.60^{-2} |
| 4–6 | 3.98^{-2} | 0.87 | 4.51^{-2} | 3.86^{-2} | 3.82^{-2} |
| 4–9 | 2.13^{-1} | 1.02 | 1.99^{-1} | 2.24^{-1} | 1.96^{-1} |
| 4–11 | 2.37^{-1} | 0.88 | 2.27^{-1} | 2.07^{-1} | 2.13^{-1} |
| 4–14 | 1.98^{-1} | 0.80 | 1.95^{-1} | 2.12^{-1} | 2.22^{-1} |
| 5–6 | 5.06^{-3} | 0.81 | 4.86^{-3} | 3.81^{-3} | 5.84^{-3} |
| 5–8 | 1.46^{-2} | 1.04 | 7.84^{-3} | 1.39^{-2} | 9.49^{-3} |
| 5–9 | 1.23^{-3} | 1.03 | 1.68^{-3} | 7.85^{-4} | 1.66^{-3} |
| 5–10 | 4.89^{-1} | 1.02 | 3.05^{-1} | 4.50^{-1} | 4.13^{-1} |
| 5–11 | 3.39^{-1} | 0.99 | 3.11^{-1} | 3.65^{-1} | 3.73^{-1} |
| 5–12 | 6.25^{-1} | 0.96 | 7.63^{-1} | 6.61^{-1} | 6.83^{-1} |
| 5–13 | 1.39^{-2} | 0.84 | 1.24^{-2} | 1.14^{-2} | 1.44^{-2} |
| 5–14 | 3.24^{-1} | 0.92 | 2.83^{-1} | 2.96^{-1} | 2.79^{-1} |
| 5–15 | 3.80^{-1} | 0.68 | 5.80^{-1} | 3.96^{-1} | 3.31^{-1} |

Notes. Index number corresponds to that in Table 2.^(a) Data in CHIANTI are from the work of Bhatia et al. (1985). ^(b) MCHF data is from the website: <http://atoms.vuse.vanderbilt.edu/> ^(c) x^y denotes $x \times 10^y$.

For Ar^{8+} , our AS agreement is within 20% when compared with that of Zhang et al. (1987) for 70% of their transitions. The percentage of all-type transition increases up to 78% with $|1.0 - gf_v/gf_L| \leq 20\%$ for this ion. As shown in Table 5, our AS results also show good agreement when compared with the results of FAC and MCHF calculations.

For Ca^{10+} , there are about 76% of transitions with a gf difference within 20% when compared with the data of Zhang et al. (1987). The difference of the present AS gf -values between the velocity and length gauges is also within 20% for 78% of all-type transitions. The comparison with results from the FAC and MCHF methods also shows good agreement, see Table 7.

For Fe^{16+} , there are about 80% of all-type transitions with $|1.0 - gf_v/gf_L| \leq 20\%$. The percentage is 67% of all available transitions from CHIANTI v6 (Dere et al. 2009) with a difference within 20% when compared with those of Landi & Gu (2006). In comparison with results of Aggarwal et al. (2003) from the MCDF method, the percentage is 65%. For the two

³ <http://open.adas.ac.uk/>

⁴ <http://atoms.vuse.vanderbilt.edu/>

⁵ The percentage refers to the fraction of transitions from the 5 lowest-lying levels to all upper states contained within the cited references.

Table 4. The level energies (Ryd) of Ar⁸⁺ from different calculations along with the compilation of NIST v3 and CHIANTI v6.

| ID | Level specification | NIST/CHIANTI ^a | AS | FAC | CHIANTI ^b | MCHF ^c |
|----|--|---------------------------|---------|---------|----------------------|-------------------|
| 1 | 2s ² 2p ⁶ 1S ₀ | | 0.00000 | | | |
| 2 | 2s ² 2p ⁵ 3s 3P ₂ | 18.4672 | 18.4701 | 18.4879 | 18.4267 | 18.4745 |
| 3 | 2s ² 2p ⁵ 3s 3P ₁ | 18.5271 | 18.5316 | 18.5510 | 18.4823 | 18.5346 |
| 4 | 2s ² 2p ⁵ 3s 3P ₀ | 18.6307 | 18.6318 | 18.6492 | 18.5898 | 18.6377 |
| 5 | 2s ² 2p ⁵ 3s 1P ₁ | 18.6967 | 18.7031 | 18.7249 | 18.6463 | 18.7045 |
| 6 | 2s ² 2p ⁵ 3p 3S ₁ | 19.5859 | 19.5907 | 19.6006 | 19.5898 | 19.6043 |
| 7 | 2s ² 2p ⁵ 3p 3D ₃ | 19.7739 | 19.7862 | 19.8001 | 19.7404 | 19.7945 |
| 8 | 2s ² 2p ⁵ 3p 3D ₂ | 19.7826 | 19.7955 | 19.8113 | 19.7475 | 19.8025 |
| 9 | 2s ² 2p ⁵ 3p 3D ₁ | 19.8049 | 19.8493 | 19.8647 | 19.7960 | 19.8549 |
| 10 | 2s ² 2p ⁵ 3p 3P ₂ | 19.8855 | 19.8968 | 19.9149 | 19.8358 | 19.9050 |
| 11 | 2s ² 2p ⁵ 3p 3P ₁ | 19.9489 | 19.9644 | 19.9775 | 19.9104 | 19.9965 |
| 12 | 2s ² 2p ⁵ 3p 3P ₀ | 19.9751 | 19.9910 | 20.0055 | 19.9271 | 20.0314 |
| 13 | 2s ² 2p ⁵ 3p 1D ₂ | 20.0026 | 20.0131 | 20.0305 | 19.9587 | 19.9685 |
| 14 | 2s ² 2p ⁵ 3p 3P ₁ | 20.0104 | 20.0245 | 20.0413 | 19.9645 | 20.0225 |
| 15 | 2s ² 2p ⁵ 3p 1S ₀ | 20.7851 | 20.7670 | 20.8484 | 20.6289 | 20.6624 |
| 16 | 2s ² 2p ⁵ 3d 3P ₀ | 21.4090 | 21.4282 | 21.4273 | 21.3865 | 21.4359 |
| 17 | 2s ² 2p ⁵ 3d 3P ₁ | 21.4276 | 21.4478 | 21.4451 | 21.4038 | 21.4539 |
| 18 | 2s ² 2p ⁵ 3d 3P ₂ | 21.4650 | 21.4876 | 21.4831 | 21.4403 | 21.4914 |
| 19 | 2s ² 2p ⁵ 3d 3F ₄ | 21.4945 | 21.5229 | 21.5169 | 21.4640 | 21.5230 |
| 20 | 2s ² 2p ⁵ 3d 3F ₃ | 21.5215 | 21.5488 | 21.5475 | 21.4885 | 21.5496 |
| 21 | 2s ² 2p ⁵ 3d 3F ₂ | 21.5794 | 21.5962 | 21.5951 | 21.5314 | 21.5962 |
| 22 | 2s ² 2p ⁵ 3d 1F ₃ | 21.6027 | 21.6352 | 21.6325 | 21.5614 | 21.6305 |
| 23 | 2s ² 2p ⁵ 3d 3D ₁ | 21.6963 | 21.7272 | 21.7266 | 21.6480 | 21.7240 |
| 24 | 2s ² 2p ⁵ 3d 1D ₂ | 21.7091 | 21.7380 | 21.7358 | 21.6690 | 21.7594 |
| 25 | 2s ² 2p ⁵ 3d 3D ₃ | 21.7312 | 21.7616 | 21.7594 | 21.6918 | 21.7622 |
| 26 | 2s ² 2p ⁵ 3d 3D ₂ | 21.7334 | 21.7652 | 21.7632 | 21.6909 | 21.7367 |
| 27 | 2s ² 2p ⁵ 3d 1P ₁ | 21.9709 | 22.0317 | 22.0372 | 21.9433 | 22.0010 |
| 28 | 2s2p ⁶ 3s 3S ₁ | | 24.2031 | 24.2183 | 24.1764 | 24.6381 |
| 29 | 2s2p ⁶ 3s 1S ₀ | | 24.4742 | 24.4911 | 24.4184 | 24.7995 |
| 30 | 2s ² 2p ⁵ 4s 3P ₂ | 24.6131 | 24.6443 | 24.6311 | 24.5969 | 24.8207 |
| 31 | 2s ² 2p ⁵ 4s 1P ₁ | 24.6402 | 24.6718 | 24.6630 | 24.6187 | 24.6671 |
| 32 | 2s ² 2p ⁵ 4s 3P ₀ | 24.7794 | 24.8031 | 24.7905 | 24.7609 | |
| 33 | 2s ² 2p ⁵ 4s 3P ₁ | 24.7936 | 24.8230 | 24.8145 | 24.7746 | |
| 34 | 2s ² 2p ⁵ 4p 3S ₁ | 25.1071 | 25.1267 | 25.1214 | 25.0596 | |
| 35 | 2s ² 2p ⁵ 4p 3D ₃ | 25.1591 | 25.1444 | 25.1408 | 25.0981 | |
| 36 | 2s ² 2p ⁵ 4p 3D ₂ | 25.1472 | 25.1500 | 25.1479 | 25.1014 | |
| 37 | 2s ² 2p ⁵ 4p 1P ₁ | 25.1598 | 25.1727 | 25.1722 | 25.1203 | |
| 38 | 2s ² 2p ⁵ 4p 3P ₂ | 25.1817 | 25.1843 | 25.1849 | 25.1307 | |
| 39 | 2s ² 2p ⁵ 4p 3P ₀ | 25.2565 | 25.2714 | 25.2739 | 25.2097 | |
| 40 | 2s ² 2p ⁵ 4p 3D ₁ | 25.3016 | 25.3050 | 25.3021 | 25.2590 | |
| 41 | 2s ² 2p ⁵ 4p 1D ₂ | 25.3225 | 25.3263 | 25.3258 | 25.2787 | |
| 42 | 2s ² 2p ⁵ 4p 3P ₁ | 25.3253 | 25.3285 | 25.3284 | 25.2750 | |
| 43 | 2s2p ⁶ 3p 3P ₀ | | 25.5061 | 25.5425 | 25.4653 | |
| 44 | 2s2p ⁶ 3p 3P ₁ | 25.3515 | 25.5140 | 25.5497 | 25.4727 | |
| 45 | 2s2p ⁶ 3p 3P ₂ | | 25.5355 | 25.5696 | 25.4927 | |
| 46 | 2s ² 2p ⁵ 4p 1S ₀ | 25.5795 | 25.5741 | 25.6269 | 25.4414 | |
| 47 | 2s2p ⁶ 3p 1P ₁ | 25.4298 | 25.6165 | 25.6467 | 25.5656 | |
| 48 | 2s ² 2p ⁵ 4d 3P ₀ | 25.7158 | 25.7514 | 25.7320 | 25.6922 | |
| 49 | 2s ² 2p ⁵ 4d 3P ₁ | 25.7260 | 25.7622 | 25.7427 | 25.7023 | |
| 50 | 2s ² 2p ⁵ 4d 3F ₄ | 25.7417 | 25.7728 | 25.7537 | 25.7187 | |
| 51 | 2s ² 2p ⁵ 4d 3P ₂ | 25.7448 | 25.7801 | 25.7607 | 25.7205 | |
| 52 | 2s ² 2p ⁵ 4d 3F ₃ | 25.7552 | 25.7857 | 25.7692 | 25.7305 | |
| 53 | 2s ² 2p ⁵ 4d 1D ₂ | 25.7753 | 25.8057 | 25.7905 | 25.7478 | |
| 54 | 2s ² 2p ⁵ 4d 3D ₃ | 25.7859 | 25.8163 | 25.8009 | 25.7560 | |
| 55 | 2s ² 2p ⁵ 4d 3D ₁ | 25.8443 | 25.8824 | 25.8706 | 25.8135 | |
| 56 | 2s ² 2p ⁵ 4d 3F ₂ | 25.9173 | 25.9460 | 25.9300 | 25.8927 | |
| 57 | 2s ² 2p ⁵ 4d 3D ₂ | 25.9255 | 25.9546 | 25.9383 | 25.8973 | |
| 58 | 2s ² 2p ⁵ 4d 1F ₃ | 25.9312 | 25.9595 | 25.9439 | 25.9037 | |
| 59 | 2s ² 2p ⁵ 4f 3D ₁ | 25.9443 | 25.9702 | 25.9638 | 25.9250 | |
| 60 | 2s ² 2p ⁵ 4f 3D ₂ | 25.9487 | 25.9754 | 25.9693 | 25.9276 | |

Notes. ^(a) Sources of NIST v3 are from the unpublished work of Shirai et al. (1999), and references therein, while that of CHIANTI v6 is from the work of Lepson et al. (2003). ^(b) Theoretical energies from Zhang et al. (1987). ^(c) MCHF data available from the website: <http://atoms.vuse.vanderbilt.edu/>

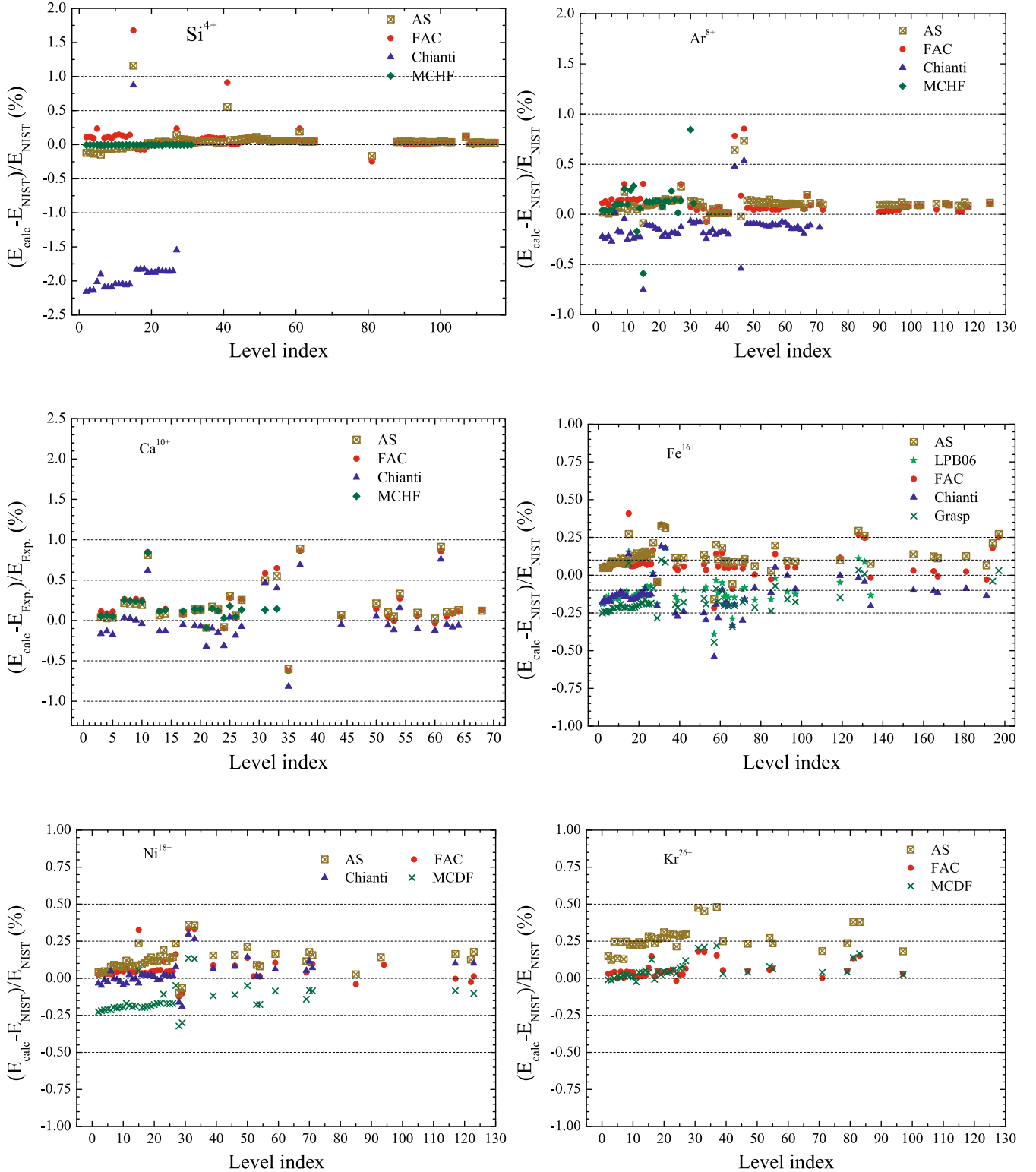


Fig. 1. Comparison of the level energies between the theoretical calculations and the “experimental” data available from NIST or CHIANTI databases. Level index refers to the ID number listed in Tables 2: Si^{4+} ; 4: Ar^{8+} ; 6: Ca^{10+} ; 8: Fe^{16+} ; 10: Ni^{18+} , and 12: Kr^{26+} . Labels in each panel corresponds to explanation in Tables of 2, 4, 8, 10, and 12, respectively. [Colour online]

key transition lines (3C and 3D), the present AS calculations (2.43 and 5.97×10^{-1}) are slightly lower than the results (2.49 and 6.39×10^{-1}) of Loch et al. 2006) by 2% and 7%, respectively, while those from Chen et al. (2003) obtained from SUPERSTRUCTURE (3C– 2.57 , 3D– 5.90×10^{-1}) and by Landi & Gu (2006) using FAC (3C– 2.52 , 3D– 5.97×10^{-1}) and the present FAC calculation are also within 7%. When pseudo-states were

included by Chen (2007) using GRASP2, it results in a slightly larger difference⁶ of $\sim 12\%$ (3C– 2.27 , 3D– 6.63×10^{-1}).

For Ni^{18+} , there are about 81% of all-type transitions showing $|1.0 - gf_v/gf_L| \leq 20\%$. When compared with results of

⁶ The MCDF level energies of Chen et al. (2003) and the A -values of Chen (2007) are used to derive the gf -values listed here.

Table 5. Comparison of the weighted oscillator strength gf between the AS and other calculations for Ar⁸⁺.

| $i - j$ | AS | | CHIANTI ^a | FAC | MCHF ^b |
|---------|---------------------|-------------|----------------------|--------------------|--------------------|
| | gf_L | gf_V/gf_L | | | |
| 1-3 | 6.75 ^{-2c} | 0.92 | 1.00 ⁻¹ | 6.76 ⁻² | 6.68 ⁻² |
| 1-5 | 1.79 ⁻¹ | 0.96 | 2.14 ⁻¹ | 1.97 ⁻¹ | 1.71 ⁻¹ |
| 1-17 | 4.41 ⁻³ | 0.96 | 5.90 ⁻³ | 4.73 ⁻³ | 4.96 ⁻³ |
| 1-23 | 1.20 ⁻¹ | 0.97 | 1.61 ⁻¹ | 1.16 ⁻¹ | 1.44 ⁻¹ |
| 1-27 | 2.06 ⁺⁰ | 0.97 | 2.55 ⁺⁰ | 2.13 ⁺⁰ | 1.89 ⁺⁰ |
| 1-33 | 2.26 ⁻² | 0.91 | 2.72 ⁻² | 3.14 ⁻² | 2.31 ⁻² |
| 1-47 | 3.63 ⁻¹ | 1.04 | 2.90 ⁻¹ | 4.12 ⁻¹ | |
| 1-55 | 9.67 ⁻² | 0.92 | 1.82 ⁻¹ | 8.28 ⁻² | |
| 1-67 | 4.96 ⁻¹ | 0.94 | 5.47 ⁻¹ | 5.40 ⁻¹ | |
| 1-181 | 1.43 ⁻³ | 0.94 | 2.50 ⁻³ | 1.43 ⁻³ | |
| 1-183 | 6.81 ⁻² | 0.98 | 1.09 ⁻¹ | 7.77 ⁻² | |
| 2-6 | 2.93 ⁻¹ | 1.02 | 2.96 ⁻¹ | 2.83 ⁻¹ | 2.91 ⁻¹ |
| 2-7 | 1.13 ⁺⁰ | 0.97 | 1.17 ⁺⁰ | 1.17 ⁺⁰ | 1.16 ⁺⁰ |
| 2-9 | 6.12 ⁻² | 0.91 | 6.67 ⁻² | 6.69 ⁻² | 6.56 ⁻² |
| 2-14 | 6.97 ⁻² | 0.80 | 8.66 ⁻² | 8.83 ⁻² | 8.60 ⁻² |
| 2-34 | 8.29 ⁻² | 1.23 | 5.84 ⁻² | 6.86 ⁻² | |
| 2-35 | 3.48 ⁻¹ | 0.98 | 3.29 ⁻¹ | 3.76 ⁻¹ | |
| 2-36 | 1.02 ⁻¹ | 1.00 | 9.44 ⁻² | 1.10 ⁻¹ | |
| 2-37 | 1.51 ⁻² | 0.98 | 1.46 ⁻² | 1.70 ⁻² | |
| 2-38 | 1.32 ⁻¹ | 1.06 | 1.15 ⁻¹ | 1.27 ⁻¹ | |
| 2-42 | 6.92 ⁻³ | 0.91 | 7.31 ⁻³ | 8.38 ⁻³ | |
| 3-6 | 7.04 ⁻² | 1.06 | 7.06 ⁻² | 7.15 ⁻² | 6.96 ⁻² |
| 3-9 | 3.87 ⁻¹ | 0.97 | 3.92 ⁻¹ | 3.80 ⁻¹ | 3.88 ⁻¹ |
| 3-10 | 2.96 ⁻¹ | 0.91 | 3.01 ⁻¹ | 3.02 ⁻¹ | 3.09 ⁻¹ |
| 3-12 | 1.52 ⁻¹ | 0.85 | 1.50 ⁻¹ | 1.54 ⁻¹ | 1.50 ⁻¹ |
| 3-13 | 7.58 ⁻² | 0.81 | 6.33 ⁻² | 7.65 ⁻² | 6.30 ⁻² |
| 3-14 | 6.62 ⁻³ | 0.61 | 7.30 ⁻³ | 8.11 ⁻³ | 7.01 ⁻³ |
| 3-15 | 6.97 ⁻² | 0.71 | 6.74 ⁻² | 6.82 ⁻² | 6.46 ⁻² |
| 3-28 | 2.35 ⁻¹ | 0.56 | 2.40 ⁻¹ | 2.41 ⁻¹ | |
| 3-29 | 4.74 ⁻² | 0.49 | 5.12 ⁻² | 4.39 ⁻² | |
| 3-34 | 4.35 ⁻³ | 1.49 | 3.69 ⁻³ | 5.02 ⁻³ | |
| 3-36 | 1.47 ⁻¹ | 0.95 | 1.37 ⁻¹ | 1.53 ⁻¹ | |
| 3-37 | 1.16 ⁻¹ | 0.98 | 1.10 ⁻¹ | 1.20 ⁻¹ | |
| 3-38 | 7.99 ⁻² | 1.02 | 7.53 ⁻² | 8.33 ⁻² | |
| 3-39 | 3.95 ⁻² | 1.06 | 3.62 ⁻² | 4.02 ⁻² | |
| 3-40 | 3.79 ⁻³ | 1.02 | 3.18 ⁻³ | 4.19 ⁻³ | |
| 3-41 | 2.59 ⁻² | 1.05 | 2.31 ⁻² | 2.89 ⁻² | |
| 3-42 | 2.82 ⁻³ | 1.57 | 2.17 ⁻³ | 3.29 ⁻³ | |
| 4-6 | 1.77 ⁻² | 1.12 | 1.77 ⁻² | 1.76 ⁻² | 1.75 ⁻² |
| 4-9 | 4.68 ⁻² | 1.10 | 3.94 ⁻² | 5.14 ⁻² | 4.28 ⁻² |
| 4-11 | 2.48 ⁻¹ | 0.95 | 2.35 ⁻¹ | 2.36 ⁻¹ | 2.30 ⁻¹ |
| 4-14 | 1.91 ⁻¹ | 0.87 | 2.12 ⁻¹ | 1.96 ⁻¹ | 2.08 ⁻¹ |
| 4-28 | 1.05 ⁻¹ | 0.57 | 1.07 ⁻¹ | 1.05 ⁻¹ | |
| 4-37 | 2.13 ⁻³ | 0.75 | 1.88 ⁻³ | 2.74 ⁻³ | |
| 4-40 | 8.14 ⁻² | 0.98 | 7.54 ⁻² | 8.54 ⁻² | |
| 4-42 | 5.35 ⁻² | 1.08 | 4.87 ⁻² | 5.60 ⁻² | |
| 5-6 | 9.51 ⁻³ | 1.12 | 1.06 ⁻² | 8.69 ⁻³ | 1.00 ⁻² |
| 5-10 | 1.04 ⁻¹ | 1.10 | 1.10 ⁻¹ | 1.04 ⁻¹ | 9.17 ⁻² |
| 5-11 | 2.25 ⁻¹ | 1.06 | 2.42 ⁻¹ | 2.32 ⁻¹ | 2.41 ⁻¹ |
| 5-12 | 3.34 ⁻² | 0.91 | 3.38 ⁻² | 3.10 ⁻² | 3.26 ⁻² |
| 5-13 | 7.29 ⁻¹ | 0.97 | 7.38 ⁻¹ | 7.28 ⁻¹ | 7.39 ⁻¹ |
| 5-14 | 2.48 ⁻¹ | 0.96 | 2.25 ⁻¹ | 2.40 ⁻¹ | 2.27 ⁻¹ |
| 5-36 | 1.13 ⁻² | 0.95 | 1.20 ⁻² | 1.17 ⁻² | |
| 5-37 | 1.49 ⁻² | 0.84 | 1.65 ⁻² | 1.61 ⁻² | |
| 5-38 | 2.49 ⁻² | 0.90 | 2.47 ⁻² | 2.81 ⁻² | |
| 5-39 | 4.04 ⁻³ | 1.08 | 4.27 ⁻³ | 4.96 ⁻³ | |
| 5-40 | 7.03 ⁻² | 0.93 | 6.73 ⁻² | 7.51 ⁻² | |
| 5-42 | 6.12 ⁻² | 1.00 | 5.91 ⁻² | 6.33 ⁻² | |
| 5-46 | 3.51 ⁻² | 1.08 | 3.36 ⁻² | 3.13 ⁻² | |

Notes. Index number corresponds to that in Table 4. ^(a) Data in CHIANTI are from the work of Zhang et al. (1987) and Hibbert et al. (1993). ^(b) MCHF data is from the website: <http://atoms.vuse.vanderbilt.edu/> ^(c) x^y denotes $x \times 10^y$.

Aggarwal & Keenan (2006), 68% of electric-dipole transitions show agreement to within 20%. The present AUTOSTRUCTURE calculations show better agreement with those from FAC (83% of transitions) and the data of Zhang et al. (1987), as currently used by CHIANTI v6 (91% of transitions).

For Kr²⁶⁺, the present results also show good agreement with previous calculations obtained using the MCDF method: Griffin et al. (2008), Rice et al. (2000) and Zhang et al. (1987), see Table 13. The ratio between the present AS gf in length and velocity gauges is within 20% of unity for 72% of all-type transitions. For the 3C and 3D lines, the present AS results are in close agreement Griffin et al's data (to within 3%).

Thus, we believe that the atomic structure of the ions spanning the sequence is reliable, and expect uncertainty on collision strengths from target structure to be small.

3. Scattering

The scattering calculations were performed using a suite of parallel intermediate-coupling frame transformation *R*-matrix codes (Griffin et al. 1998). Due to the large size of the *R*-matrix “box” (due to the 7d orbital included), we employed 60 basis orbitals to represent the ($N + 1$)th-electron continuum per angular momentum for most ions over the sequence. For lower charged ions, the basis orbitals are increased, e.g. 65 for Si⁴⁺ and P⁵⁺, 75 for Al³⁺, 85 for Mg²⁺ and 95 for Na⁺. All partial waves from $J = 1/2$ to 81/2 were included explicitly and contributions from higher J -values were included using a “top-up” procedure (Burgess 1974; Badnell & Griffin 2001). The contributions from partial waves up to $J = 23/2$ were included in the exchange *R*-matrix calculation, while those from $J = 25/2$ to 81/2 were included via a non-exchange *R*-matrix calculation. For the exchange calculation, a fine energy mesh was used to resolve the dominant resonances below the highest excitation threshold, see Table 14. From just above the highest threshold excitation to a maximum energy of 3.0 times the ionization potential for each ion, a coarse energy mesh ($2.0 \times 10^{-3} q^2$ Ryd, $q = Z - 10$ is the residual charge of ion) was employed. For the non-exchange calculation, a step of $2.0 \times 10^{-3} q^2$ Ryd was used over the entire energy range. Witthoef et al. (2007) tested the convergence of the effective strengths (Υ) with respect to resonance resolutions for several ions spanning the F-like sequence – we adopt the recommended energy meshes of Witthoef et al. (2007) or better ones, see Table 14.

We then used the infinite energy Born limits (non-dipole allowed) and line-strengths (dipole-allowed) from AUTOSTRUCTURE so that higher energy reduced collision strengths (Ω), as defined by Burgess & Tully (1992), can be found from interpolation in Burgess-Tully space for all additional higher energies. The effective collision strengths at 13 electron temperatures ranging from $2 \times 10^2 (q + 1)^2$ K to $2 \times 10^6 (q + 1)^2$ K (q is the residual charge of the ion, that is $Z - 10$), are produced as the end product. The data were stored in the ADAS adf04 format (Summers 2004).

4. Results and discussions

4.1. Comparison with previous calculations

We compare the present ICFT *R*-matrix results with those of previous works (DW and/or *R*-matrix) for three ions (Si⁴⁺, Fe¹⁶⁺ and Kr²⁶⁺) which span the calculated data for this iso-electronic

Table 6. The level energies (Ryd) of Ca¹⁰⁺ from different calculations along with experimental data compiled in CHIANTI v6.

| ID | level specification | Exp. ^a | AS | FAC | CHIANTI ^b | MCHF ^c |
|----|--|-------------------|---------|---------|----------------------|-------------------|
| 1 | 2s ² 2p6 ¹ S ₀ | | 0.0000 | 0.0000 | 0.0000 | 0.0000 |
| 2 | 2s ² 2p ⁵ 3s ³ P ₂ | | 25.5427 | 25.5586 | 25.4991 | 25.5486 |
| 3 | 2s ² 2p ⁵ 3s ³ P ₁ | 25.6149 | 25.6249 | 25.6435 | 25.5729 | 25.6289 |
| 4 | 2s ² 2p ⁵ 3s ³ P ₀ | 25.8053 | 25.8126 | 25.8279 | 25.7707 | 25.8205 |
| 5 | 2s ² 2p ⁵ 3s ¹ P ₁ | 25.8791 | 25.8880 | 25.9076 | 25.8335 | 25.8924 |
| 6 | 2s ² 2p ⁵ 3p ³ S ₁ | | 26.9270 | 26.9345 | 26.9288 | 26.9431 |
| 7 | 2s ² 2p ⁵ 3p ³ D ₂ | 27.1020 | 27.1604 | 27.1738 | 27.1112 | 27.1699 |
| 8 | 2s ² 2p ⁵ 3p ³ D ₃ | 27.1075 | 27.1613 | 27.1733 | 27.1152 | 27.1738 |
| 9 | 2s ² 2p ⁵ 3p ¹ P ₁ | 27.1813 | 27.2386 | 27.2530 | 27.1819 | 27.2461 |
| 10 | 2s ² 2p ⁵ 3p ³ P ₂ | 27.2451 | 27.2975 | 27.3143 | 27.2340 | 27.3093 |
| 11 | 2s ² 2p ⁵ 3p ³ D ₁ | 27.2059 | 27.4268 | 27.4360 | 27.3743 | 27.4337 |
| 12 | 2s ² 2p ⁵ 3p ³ P ₀ | | 27.4440 | 27.4562 | 27.3768 | 27.4516 |
| 13 | 2s ² 2p ⁵ 3p ¹ D ₂ | 27.4893 | 27.5070 | 27.5222 | 27.4526 | 27.5210 |
| 14 | 2s ² 2p ⁵ 3p ³ P ₁ | 27.4884 | 27.5124 | 27.5273 | 27.4526 | 27.5239 |
| 15 | 2s ² 2p ⁵ 3p ¹ S ₀ | | 28.3886 | 28.4770 | 28.2369 | 28.2858 |
| 16 | 2s ² 2p ⁵ 3d ³ P ₀ | | 29.1508 | 29.1489 | 29.1114 | 29.1602 |
| 17 | 2s ² 2p ⁵ 3d ³ P ₁ | 29.1543 | 29.1812 | 29.1767 | 29.1387 | 29.1880 |
| 18 | 2s ² 2p ⁵ 3d ³ P ₂ | | 29.2418 | 29.2343 | 29.1934 | 29.2443 |
| 19 | 2s ² 2p ⁵ 3d ³ F ₄ | 29.2344 | 29.2760 | 29.2659 | 29.2152 | 29.2758 |
| 20 | 2s ² 2p ⁵ 3d ³ F ₃ | 29.2708 | 29.3104 | 29.3071 | 29.2499 | 29.3118 |
| 21 | 2s ² 2p ⁵ 3d ³ F ₂ | 29.4029 | 29.3772 | 29.3747 | 29.3082 | 29.3764 |
| 22 | 2s ² 2p ⁵ 3d ³ D ₃ | 29.3765 | 29.4265 | 29.4200 | 29.3474 | 29.4200 |
| 23 | 2s ² 2p ⁵ 3d ³ D ₁ | 29.5224 | 29.5622 | 29.5594 | 29.4777 | 29.5577 |
| 24 | 2s ² 2p ⁵ 3d ¹ D ₂ | 29.6271 | 29.6026 | 29.5980 | 29.5342 | 29.6361 |
| 25 | 2s ² 2p ⁵ 3d ³ D ₂ | 29.5506 | 29.6395 | 29.6338 | 29.5624 | 29.6030 |
| 26 | 2s ² 2p ⁵ 3d ¹ F ₃ | 29.6253 | 29.6428 | 29.6366 | 29.5707 | 29.6402 |
| 27 | 2s ² 2p ⁵ 3d ¹ P ₁ | 29.9288 | 30.0051 | 30.0059 | 29.9060 | 29.9684 |
| 28 | 2s2p ⁶ 3s ³ S ₁ | | 32.2654 | 32.2832 | 32.2261 | |
| 29 | 2s2p ⁶ 3s ¹ S ₀ | | 32.5841 | 32.6044 | 32.5190 | |
| 30 | 2s2p ⁶ 3p ³ P ₀ | | 33.8113 | 33.8432 | 33.7971 | 33.6845 |
| 31 | 2s2p ⁶ 3p ³ P ₁ | 33.6523 | 33.8206 | 33.8495 | 33.8090 | 33.6960 |
| 32 | 2s2p ⁶ 3p ³ P ₂ | | 33.8508 | 33.8733 | 33.8464 | 33.7327 |
| 33 | 2s2p ⁶ 3p ¹ P ₁ | 33.7981 | 33.9839 | 34.0176 | 33.9338 | 33.8469 |
| 34 | 2s ² 2p ⁵ 4s ³ P ₂ | | 34.2467 | 34.2404 | 34.1543 | |
| 35 | 2s ² 2p ⁵ 4s ¹ P ₁ | 34.4633 | 34.2563 | 34.2488 | 34.1817 | |
| 36 | 2s ² 2p ⁵ 4s ³ P ₀ | | 34.5012 | 34.4901 | 34.4277 | |
| 37 | 2s ² 2p ⁵ 4s ³ P ₁ | 34.2082 | 34.5124 | 34.5026 | 34.4432 | |
| 38 | 2s ² 2p ⁵ 4p ³ S ₁ | | 34.7857 | 34.7746 | 34.7320 | |
| 39 | 2s ² 2p ⁵ 4p ³ D ₃ | | 34.8251 | 34.8174 | 34.7818 | |
| 40 | 2s ² 2p ⁵ 4p ³ D ₂ | | 34.8270 | 34.8207 | 34.7802 | |
| 41 | 2s ² 2p ⁵ 4p ¹ P ₁ | | 34.8601 | 34.8562 | 34.8074 | |
| 42 | 2s ² 2p ⁵ 4p ³ P ₂ | | 34.8770 | 34.8745 | 34.8230 | |
| 43 | 2s ² 2p ⁵ 4p ³ P ₀ | | 35.0069 | 35.0089 | 34.9386 | |
| 44 | 2s ² 2p ⁵ 4p ³ D ₁ | 35.0628 | 35.0862 | 35.0788 | 35.0446 | |
| 45 | 2s ² 2p ⁵ 4p ¹ D ₂ | | 35.1190 | 35.1149 | 35.0754 | |
| 46 | 2s ² 2p ⁵ 4p ³ P ₁ | | 35.1201 | 35.1165 | 35.0691 | |
| 47 | 2s ² 2p ⁵ 4p ¹ S ₀ | | 35.3734 | 35.4243 | 35.2506 | |
| 48 | 2s ² 2p ⁵ 4d ³ P ₀ | | 35.5595 | 35.5355 | 35.5085 | |
| 49 | 2s ² 2p ⁵ 4d ³ P ₁ | | 35.5757 | 35.5516 | 35.5230 | |
| 50 | 2s ² 2p ⁵ 4d ³ F ₄ | 35.5245 | 35.5992 | 35.5751 | 35.5431 | |
| 51 | 2s ² 2p ⁵ 4d ³ P ₂ | | 35.6032 | 35.5793 | 35.5477 | |
| 52 | 2s ² 2p ⁵ 4d ³ F ₃ | 35.5799 | 35.6149 | 35.5945 | 35.5586 | |
| 53 | 2s ² 2p ⁵ 4d ¹ D ₂ | 35.6233 | 35.6407 | 35.6217 | 35.5814 | |
| 54 | 2s ² 2p ⁵ 4d ³ D ₃ | 35.5377 | 35.6551 | 35.6352 | 35.5932 | |
| 55 | 2s ² 2p ⁵ 4f ³ D ₁ | | 35.7173 | 35.7076 | 35.8297 | |
| 56 | 2s ² 2p ⁵ 4f ³ D ₂ | | 36.1749 | 35.7228 | 35.8340 | |
| 57 | 2s ² 2p ⁵ 4d ³ D ₁ | 35.7126 | 35.7469 | 35.7315 | 35.6752 | |
| 58 | 2s ² 2p ⁶ 3d ³ D ₃ | | 35.7674 | 35.7553 | 35.9009 | |
| 59 | 2s ² 2p ⁵ 4f ¹ D ₂ | | 35.7339 | 35.8565 | 35.8347 | |
| 60 | 2s ² 2p ⁵ 4d ³ F ₂ | 35.8730 | 35.8811 | 35.8612 | 35.8283 | |

Notes. ^(a) Experimental data are from the CHIANTI v6 database – see references therein. ^(b) Theoretical energies from Zhang et al. (1987). ^(c) MCHF data is available from the website: <http://atoms.vuse.vanderbilt.edu/>

sequence. Here, we select the extensively studied transition line $3D$ as a sensitive test of the accuracy of the present ICFT *R*-matrix calculation, and give special attention to the cosmic abundant ion- Fe^{16+} . (The $3C$ line is less sensitive to the collision method because its excitation is more strongly non-resonant, but we show a comparison with experiment for Fe^{16+} along with $3D$.) An extensive comparison (all available excitation data from ground state $2s^2 2p^6 \ ^1S_0$) between the present ICFT *R*-matrix and previous calculations (with preference to data with resonances included) has been made for the three ions to test widespread of accuracy of the present ICFT *R*-matrix data.

— Si^{4+} To our best knowledge, there is no *R*-matrix data available. The DW data of (Bhatia et al. 1985, with only ground and $2s^2 2p^5 3l$ configurations included) was extensively used by current modelling codes, including CHIANTI v6. For the $3D$ line as shown in Fig. 2, the data from the DW calculations (Bhatia et al. (1985) at $E_e = 204.09$ eV, and the present FAC calculation) agrees with the background cross-section (σ) of the present ICFT *R*-matrix calculation to within 20%. Below the electron energy of $E_e = 150$ eV, the data of FAC is slightly higher than the background of the present ICFT *R*-matrix calculation. At low temperatures $T_e < 1.0 \times 10^5$ K, the present ICFT Υ is higher than that of Bhatia et al. (1985) by $\sim 80\%$, however, it is in agreement with the FAC calculation. At the temperature ($T_e = 1.6 \times 10^5$ K) with peak abundance in ionization equilibrium (Mazzotta et al. 1998; Bryans et al. 2006); Bhatia et al.'s data is lower than the present ICFT data by $\sim 40\%$. The FAC result shows an excellent agreement with the present ICFT result. Above the temperature of $T_e = 1.0 \times 10^6$ K, the difference between the present Υ and the result of Bhatia et al. (1985) is about $\sim 45\%$. This is higher than the general assessment criteria for the $3D$ transition as in cases of Fe^{16+} and Kr^{26+} discussed at following. This discrepancy at high temperatures is due to lower cross-sections from the DW calculation at high energies where the line strength (S) dominates the cross-section. This is consistent with the difference of the collision strength limit $4gf/E_{ij} = 4S/3$ for this transition (AS: 3.39×10^{-2} ; FAC: 2.65×10^{-2} ; Bhatia et al. 1985: 2.84×10^{-2} , MCHF⁴: 4.39×10^{-2} , see Table 3). The present AS calculation is within the range of the low (FAC) and high (MCHF) cases. Moreover, the excellent agreement of level energies between the present AUTOSTRUCTURE calculation and NIST data give more confidence to the present ICFT *R*-matrix calculation.

An extensive comparison with the results of Bhatia et al. (1985) is made in Fig. 3. At a low temperature of $T_e = 2.5 \times 10^4$ K, all available excitation data (DW) of Bhatia et al. (1985) from the ground state is lower than the present ICFT *R*-matrix calculation, and only 4% of them are within 20%. At the temperature (1.6×10^5 K) of peak fractional abundance in ionization equilibrium (Mazzotta et al. 1998; Bryans et al. 2006), the percentage increases to 19%. At a high temperature of $T_e = 2.5 \times 10^6$ K, 50% of excitations from the ground state show agreement to within 20%.

— Fe^{16+} Many calculations have been done with resonances taken into account, such as the serial work of Chen et al. (2003, 2006), Chen (2007), Aggarwal et al. (2003), Loch et al. (2006), and Landi & Gu (2006). In Fig. 4, we present the comparison of cross-sections and effective collision strengths Υ with previous available data, for the $3D$ -excitation (1–23). In the work of Loch et al. (2006), a finer energy mesh of about 10 times present case was employed to test the convergence of the Υ relative to the resolution of resonances. They concluded that the effect is quite small when compared with their results obtained with a coarser energy mesh (20 000 points in the

Table 7. Comparison of the weighted oscillator strength gf between the AS and other calculations for Ca^{10+} .

| $i - j$ | AS | | CHIANTI ^(a) | FAC | MCHF ^(b) |
|---------|-------------|-------------|------------------------|-------------|---------------------|
| | gf_L | gf_V/gf_L | | | |
| 1–3 | 9.05^{-2} | 0.93 | 1.09^{-1} | 9.16^{-2} | 8.77^{-2} |
| 1–5 | 1.50^{-1} | 0.96 | 1.60^{-1} | 1.64^{-1} | 1.46^{-1} |
| 1–17 | 5.74^{-3} | 0.97 | 7.20^{-3} | 6.29^{-3} | 6.44^{-3} |
| 1–23 | 1.86^{-1} | 0.98 | 2.34^{-1} | 1.85^{-1} | 2.17^{-1} |
| 1–27 | 2.29^{+0} | 0.98 | 2.68^{+0} | 2.35^{+0} | 2.12^{+0} |
| 1–31 | 1.00^{-2} | 0.98 | 1.07^{-2} | 1.04^{-2} | 9.10^{-3} |
| 1–33 | 2.94^{-1} | 1.05 | 3.10^{-1} | 3.11^{-1} | 2.70^{-1} |
| 1–35 | 1.04^{-2} | 0.76 | 3.09^{-2} | 1.23^{-2} | |
| 1–37 | 8.93^{-3} | 0.87 | 2.26^{-2} | 1.22^{-2} | |
| 1–49 | 3.25^{-3} | 0.94 | 3.70^{-3} | 3.65^{-3} | |
| 1–181 | 2.13^{-3} | 0.96 | 5.10^{-3} | 2.39^{-3} | |
| 1–183 | 6.46^{-2} | 0.99 | 1.14^{-1} | 7.17^{-2} | |
| 2–6 | 2.72^{-1} | 1.07 | 2.78^{-1} | 2.68^{-1} | 2.75^{-1} |
| 2–7 | 3.16^{-1} | 0.97 | 3.15^{-1} | 3.21^{-1} | 3.18^{-1} |
| 2–8 | 1.04^{+0} | 0.97 | 1.04^{+0} | 1.04^{+0} | 1.03^{+0} |
| 2–9 | 5.83^{-2} | 0.93 | 5.62^{-2} | 5.86^{-2} | 5.61^{-2} |
| 2–13 | 2.90^{-2} | 0.75 | 3.03^{-2} | 2.89^{-2} | 2.66^{-2} |
| 2–14 | 6.45^{-2} | 0.80 | 6.40^{-2} | 6.54^{-2} | 6.25^{-2} |
| 2–38 | 1.38^{-1} | 1.04 | 4.71^{-1} | 1.43^{-1} | |
| 2–39 | 4.24^{-1} | 0.98 | 3.93^{-1} | 4.43^{-1} | |
| 2–41 | 1.53^{-2} | 1.00 | 1.46^{-2} | 1.68^{-2} | |
| 2–42 | 1.55^{-1} | 1.04 | 1.44^{-1} | 1.57^{-1} | |
| 2–46 | 4.06^{-3} | 1.07 | 3.79^{-3} | 4.56^{-3} | |
| 3–6 | 4.84^{-2} | 1.12 | 4.89^{-2} | 4.92^{-2} | 4.79^{-2} |
| 3–7 | 4.06^{-1} | 1.04 | 4.07^{-1} | 3.99^{-1} | 3.99^{-1} |
| 3–9 | 3.70^{-1} | 1.00 | 3.71^{-1} | 3.67^{-1} | 4.01^{-1} |
| 3–11 | 6.55^{-3} | 1.01 | 4.90^{-3} | 6.92^{-3} | 5.33^{-3} |
| 3–12 | 1.26^{-1} | 0.86 | 1.26^{-1} | 1.27^{-1} | 1.26^{-1} |
| 3–13 | 3.51^{-2} | 0.79 | 2.91^{-2} | 3.66^{-2} | 2.98^{-2} |
| 3–14 | 1.27^{-3} | 0.44 | 1.90^{-3} | 1.76^{-3} | 1.52^{-3} |
| 3–15 | 8.37^{-2} | 0.72 | 7.95^{-2} | 8.36^{-2} | 7.66^{-2} |
| 3–28 | 1.71^{-1} | 0.52 | 1.77^{-1} | 1.75^{-1} | |
| 3–29 | 6.18^{-2} | 0.47 | 6.58^{-2} | 5.85^{-2} | |
| 3–38 | 1.38^{-2} | 1.03 | 1.33^{-2} | 1.56^{-2} | |
| 3–41 | 1.54^{-1} | 0.97 | 1.46^{-1} | 1.59^{-1} | |
| 3–42 | 1.07^{-1} | 1.01 | 1.01^{-1} | 1.11^{-1} | |
| 3–43 | 4.56^{-2} | 1.05 | 4.21^{-2} | 4.59^{-2} | |
| 3–44 | 2.42^{-3} | 1.03 | 2.04^{-3} | 2.67^{-3} | |
| 3–46 | 2.33^{-3} | 1.33 | 1.96^{-3} | 2.71^{-3} | |
| 4–6 | 1.12^{-2} | 1.25 | 1.12^{-2} | 1.12^{-2} | 1.11^{-2} |
| 4–11 | 2.20^{-1} | 0.98 | 2.05^{-1} | 2.13^{-1} | 2.05^{-1} |
| 4–14 | 1.97^{-1} | 0.90 | 2.14^{-1} | 2.01^{-1} | 2.11^{-1} |
| 4–28 | 8.84^{-2} | 0.55 | 9.12^{-2} | 8.79^{-2} | |
| 4–38 | 1.35^{-3} | 0.99 | 1.18^{-3} | 1.69^{-3} | |
| 4–41 | 1.20^{-3} | 0.75 | 1.09^{-3} | 1.54^{-3} | |
| 4–44 | 9.03^{-2} | 0.97 | 8.44^{-2} | 9.45^{-2} | |
| 4–46 | 7.91^{-2} | 1.03 | 7.27^{-2} | 8.16^{-2} | |
| 4–55 | 2.18^{-3} | 0.93 | 2.18^{-3} | 2.41^{-3} | |
| 5–6 | 9.03^{-3} | 1.26 | 9.60^{-3} | 8.52^{-3} | 9.20^{-3} |
| 5–11 | 2.06^{-1} | 1.08 | 2.20^{-1} | 2.09^{-1} | 2.18^{-1} |
| 5–12 | 3.89^{-2} | 0.94 | 3.80^{-2} | 3.71^{-2} | 3.71^{-2} |
| 5–13 | 7.01^{-1} | 0.98 | 7.04^{-1} | 6.99^{-1} | 7.03^{-1} |
| 5–14 | 2.10^{-1} | 0.98 | 1.92^{-1} | 2.05^{-1} | 1.94^{-1} |
| 5–15 | 1.96^{-1} | 0.75 | 1.87^{-1} | 2.06^{-1} | 1.86^{-1} |
| 5–28 | 9.73^{-2} | 0.56 | 9.89^{-2} | 9.26^{-2} | |
| 5–29 | 1.01^{-1} | 0.52 | 1.10^{-1} | 9.97^{-2} | |
| 5–41 | 8.93^{-3} | 0.83 | 1.02^{-2} | 9.82^{-3} | |
| 5–44 | 9.30^{-2} | 0.94 | 8.84^{-2} | 9.78^{-2} | |
| 5–45 | 2.80^{-1} | 0.98 | 2.64^{-1} | 2.89^{-1} | |
| 5–46 | 7.79^{-2} | 0.99 | 7.52^{-2} | 8.07^{-2} | |
| 5–47 | 3.92^{-2} | 1.10 | 3.63^{-2} | 3.62^{-2} | |

Notes. Index number corresponds to that in Table 6. ^(a) Data in CHIANTI from the work of Zhang et al. (1987) and Hibbert et al. (1993). ^(b) Data is calculated with multiconfiguration Hartree-Fock (MCHF) or multiconfiguration Dirac-Fock (MCDF) method, and available from the website: <http://atoms.vuse.vanderbilt.edu/> ^(c) x^y denotes $x \times 10^y$.

Table 8. The level energies (Ryd) of Fe¹⁶⁺ from different calculations along with the compilation of NIST v3.

| ID | Level specification | NIST ^a | AS | FAC | MCDF ^b | CHIANTI ^c | LPB06 ^d |
|----|--|-------------------|---------|---------|-------------------|----------------------|--------------------|
| 1 | 2s ² 2p ⁶ 1S ₀ | | | | | | |
| 2 | 2s ² 2p ⁵ 3s 3P ₂ | 53.3045 | 53.3307 | 53.3312 | 53.1706 | 53.2094 | 53.2031 |
| 3 | 2s ² 2p ⁵ 3s 1P ₁ | 53.4437 | 53.4689 | 53.4779 | 53.3143 | 53.3568 | 53.3448 |
| 4 | 2s ² 2p ⁵ 3s 3P ₀ | 54.2314 | 54.2578 | 54.2560 | 54.0986 | 54.1357 | 54.1517 |
| 5 | 2s ² 2p ⁵ 3s 3P ₁ | 54.3194 | 54.3462 | 54.3496 | 54.1897 | 54.2300 | 54.2431 |
| 6 | 2s ² 2p ⁵ 3p 3S ₁ | 55.5276 | 55.5708 | 55.5563 | 55.3951 | 55.4308 | 55.4328 |
| 7 | 2s ² 2p ⁵ 3p 3D ₂ | 55.7849 | 55.8376 | 55.8272 | 55.6636 | 55.7067 | 55.6964 |
| 8 | 2s ² 2p ⁵ 3p 3D ₃ | 55.9038 | 55.9520 | 55.9426 | 55.7804 | 55.8246 | 55.8201 |
| 9 | 2s ² 2p ⁵ 3p 1P ₁ | 55.9869 | 56.0364 | 56.0320 | 55.8682 | 55.9135 | 55.9022 |
| 10 | 2s ² 2p ⁵ 3p 3P ₂ | 56.1201 | 56.1639 | 56.1619 | 55.9989 | 56.0474 | 56.0335 |
| 11 | 2s ² 2p ⁵ 3p 3P ₀ | 56.5191 | 56.5849 | 56.5719 | 56.4098 | 56.4579 | 56.4508 |
| 12 | 2s ² 2p ⁵ 3p 3D ₁ | 56.6718 | 56.7311 | 56.7111 | 56.5526 | 56.6006 | 56.6084 |
| 13 | 2s ² 2p ⁵ 3p 3P ₁ | 56.9105 | 56.9573 | 56.9494 | 56.7885 | 56.8289 | 56.8445 |
| 14 | 2s ² 2p ⁵ 3p 1D ₂ | 56.9383 | 56.9872 | 56.9778 | 56.8171 | 56.8582 | 56.8772 |
| 15 | 2s ² 2p ⁵ 3p 1S ₀ | 57.8965 | 58.0542 | 58.1335 | 57.9419 | 57.9776 | 57.9856 |
| 16 | 2s ² 2p ⁵ 3d 3P ₀ | 58.9041 | 58.9616 | 58.9393 | 58.7755 | 58.8068 | 58.8127 |
| 17 | 2s ² 2p ⁵ 3d 3P ₁ | 58.9754 | 59.0393 | 59.0102 | 58.8470 | 58.8790 | 58.8896 |
| 18 | 2s ² 2p ⁵ 3d 3P ₂ | 59.1084 | 59.1836 | 59.1458 | 58.9838 | 59.0170 | 59.0303 |
| 19 | 2s ² 2p ⁵ 3d 3F ₄ | 59.1123 | 59.1979 | 59.1518 | 58.9913 | 59.0242 | 59.0417 |
| 20 | 2s ² 2p ⁵ 3d 3F ₃ | 59.1688 | 59.2402 | 59.2122 | 59.0521 | 59.0874 | 59.0991 |
| 21 | 2s ² 2p ⁵ 3d 1D ₂ | 59.2934 | 59.3676 | 59.3423 | 59.1821 | 59.2187 | 59.2247 |
| 22 | 2s ² 2p ⁵ 3d 3D ₃ | 59.3722 | 59.4603 | 59.4210 | 59.2625 | 59.3014 | 59.3077 |
| 23 | 2s ² 2p ⁵ 3d 3D ₁ | 59.7080 | 59.8023 | 59.7720 | 59.6131 | 59.6558 | 59.6588 |
| 24 | 2s ² 2p ⁵ 3d 3F ₂ | 60.0922 | 60.1639 | 60.1337 | 59.9778 | 60.0127 | 60.0446 |
| 25 | 2s ² 2p ⁵ 3d 3D ₂ | 60.1523 | 60.2362 | 60.1962 | 60.0370 | 60.0718 | 60.1031 |
| 26 | 2s ² 2p ⁵ 3d 1F ₃ | 60.1906 | 60.2777 | 60.2357 | 60.0784 | 60.1136 | 60.1476 |
| 27 | 2s ² 2p ⁵ 3d 1P ₁ | 60.6904 | 60.8214 | 60.7903 | 60.6368 | 60.6927 | 60.6979 |
| 28 | 2s2p ⁶ 3s 3S ₁ | | 63.3645 | 63.3648 | 63.2124 | 63.2696 | 63.2710 |
| 29 | 2s2p ⁶ 3s 1S ₀ | 63.8798 | 63.8515 | 63.8514 | 63.6988 | 63.7498 | 63.7572 |
| 30 | 2s2p ⁶ 3p 3P ₀ | | 65.7796 | 65.7877 | 65.6342 | 65.6924 | 65.6910 |
| 31 | 2s2p ⁶ 3p 3P ₁ | 65.6012 | 65.8153 | 65.8214 | 65.6674 | 65.7260 | 65.7266 |
| 32 | 2s2p ⁶ 3p 3P ₂ | | 65.9876 | 65.9901 | 65.8373 | 65.8944 | 65.9017 |
| 33 | 2s2p ⁶ 3p 1P ₁ | 65.9238 | 66.1298 | 66.1379 | 65.9800 | 66.0421 | 66.0427 |
| 34 | 2s2p ⁶ 3d 3D ₁ | | 69.0895 | 69.0653 | 68.9199 | 68.9602 | 68.9884 |
| 35 | 2s2p ⁶ 3d 3D ₂ | | 69.1085 | 69.0752 | 68.9299 | 68.9704 | 69.0021 |
| 36 | 2s2p ⁶ 3d 3D ₃ | | 69.1411 | 69.0942 | 68.9492 | 68.9891 | 69.0244 |
| 37 | 2s2p ⁶ 3d 1D ₂ | | 69.4869 | 69.4588 | 69.3246 | 69.3763 | 69.3962 |
| 38 | 2s ² 2p ⁵ 4s 3P ₂ | 71.7987 | 71.8811 | 71.8355 | 71.6597 | 71.6171 | 71.6967 |
| 39 | 2s ² 2p ⁵ 4s 1P ₁ | 71.8607 | 71.9220 | 71.8848 | 71.7069 | 71.6641 | 71.7432 |
| 40 | 2s ² 2p ⁵ 4p 3S ₁ | | 72.7994 | 72.7615 | 72.5911 | 72.5318 | 72.6254 |
| 41 | 2s ² 2p ⁵ 4s 3P ₀ | | 72.8081 | 72.7629 | 72.5874 | 72.5469 | 72.6500 |
| 42 | 2s ² 2p ⁵ 4s 3P ₁ | 72.7464 | 72.8295 | 72.7883 | 72.6153 | 72.5710 | 72.6746 |
| 43 | 2s ² 2p ⁵ 4p 3D ₂ | | 72.8634 | 72.8319 | 72.6530 | 72.6004 | 72.6897 |
| 44 | 2s ² 2p ⁵ 4p 3D ₃ | | 72.9087 | 72.8792 | 72.7022 | 72.6435 | 72.7416 |
| 45 | 2s ² 2p ⁵ 4p 1P ₁ | | 72.9373 | 72.9115 | 72.7323 | 72.6753 | 72.7699 |
| 46 | 2s ² 2p ⁵ 4p 3P ₂ | | 72.9786 | 72.9557 | 72.7756 | 72.7170 | 72.8132 |
| 47 | 2s ² 2p ⁵ 4p 3P ₀ | | 73.2551 | 73.2511 | 73.0634 | 72.9940 | 73.1028 |
| 48 | 2s ² 2p ⁵ 4p 3D ₁ | | 73.7730 | 73.7383 | 73.5649 | 73.5003 | 73.6243 |
| 49 | 2s ² 2p ⁵ 4p 3P ₁ | | 73.8526 | 73.8255 | 73.6515 | 73.5963 | 73.7118 |
| 50 | 2s ² 2p ⁵ 4p 1D ₂ | | 73.8697 | 73.8431 | 73.6682 | 73.6135 | 73.7296 |
| 51 | 2s ² 2p ⁵ 4d 3P ₀ | | 74.0252 | 73.9790 | 73.8125 | 73.7417 | 73.8512 |
| 52 | 2s ² 2p ⁵ 4d 3P ₁ | 73.9584 | 74.0590 | 74.0119 | 73.8449 | 73.7727 | 73.8853 |
| 53 | 2s ² 2p ⁵ 4d 3F ₄ | 74.0277 | 74.1043 | 74.1091 | 73.8853 | 73.8308 | 73.9701 |
| 54 | 2s ² 2p ⁵ 4p 1S ₀ | | 74.0833 | 74.0531 | 73.9148 | 73.8083 | 73.9491 |
| 55 | 2s ² 2p ⁵ 4d 3P ₂ | | 74.1140 | 74.0660 | 73.8982 | 73.8224 | 73.9396 |
| 56 | 2s ² 2p ⁵ 4d 3F ₃ | | 74.1195 | 74.0767 | 73.9075 | 73.8364 | 73.9283 |
| 57 | 2s ² 2p ⁵ 4d 1D ₂ | 74.2838 | 74.1644 | 74.1236 | 73.9538 | 73.8813 | 73.9939 |
| 58 | 2s ² 2p ⁵ 4d 3D ₃ | 74.0477 | 74.1970 | 74.1519 | 73.9819 | 73.9044 | 74.0231 |
| 59 | 2s ² 2p ⁵ 4d 3D ₁ | 74.3047 | 74.3832 | 74.3478 | 74.1765 | 74.0944 | 74.2181 |
| 60 | 2s ² 2p ⁵ 4f 3D ₁ | | 74.6746 | 74.6503 | 74.4623 | 74.4692 | 74.5017 |

Notes. ^a Sources of the NIST v3 are from the work of [Sugar & Corliss \(1985\)](#) and references therein. ^b MCDF data from the work of [Aggarwal et al. \(2004\)](#). ^c Data in CHIANTI are from the work of [Landi & Gu \(2006\)](#). ^d LPB06 corresponds to the work of [Loch et al. \(2006\)](#).

Table 9. Comparison of the weighted oscillator strength gf between the AS and other calculations for Fe^{16+} .

| $i - j$ | AS | | GRASP ^a | CHIANTI ^b | FAC | SS ^c |
|---------|--------------------|-------------|--------------------|----------------------|--------------------|--------------------|
| | gf_L | gf_V/gf_L | | | | |
| 1-3 | 1.25 ⁻¹ | 0.91 | 1.26 ⁻¹ | 1.23 ⁻¹ | 1.27 ⁻¹ | 1.24 ⁻¹ |
| 1-5 | 1.02 ⁻¹ | 0.97 | 1.07 ⁻¹ | 1.06 ⁻¹ | 1.10 ⁻¹ | 1.02 ⁻¹ |
| 1-17 | 8.77 ⁻³ | 0.97 | 9.94 ⁻³ | 9.96 ⁻³ | 1.01 ⁻² | 8.70 ⁻³ |
| 1-23 | 5.97 ⁻¹ | 0.99 | 6.18 ⁻¹ | 5.97 ⁻¹ | 6.09 ⁻¹ | 5.90 ⁻¹ |
| 1-27 | 2.43 ⁺⁰ | 0.99 | 2.56 ⁻⁰ | 2.52 ⁺⁰ | 2.46 ⁺⁰ | 2.57 ⁺⁰ |
| 1-31 | 3.54 ⁻² | 1.01 | 3.55 ⁻² | 3.37 ⁻² | 3.57 ⁻² | 3.15 ⁻² |
| 1-42 | 1.42 ⁻² | 0.92 | 1.84 ⁻² | 1.64 ⁻² | 1.83 ⁻² | 1.49 ⁻² |
| 1-52 | 3.41 ⁻³ | 0.95 | 3.94 ⁻³ | 4.53 ⁻³ | 4.03 ⁻³ | 3.57 ⁻³ |
| 1-59 | 3.70 ⁻¹ | 0.96 | 4.13 ⁻¹ | 3.76 ⁻¹ | 3.82 ⁻¹ | 4.08 ⁻¹ |
| 1-71 | 4.24 ⁻¹ | 0.97 | 5.10 ⁻¹ | 4.36 ⁻¹ | 4.60 ⁻¹ | 4.95 ⁻¹ |
| 1-129 | 1.25 ⁻² | 0.93 | 1.69 ⁻² | 1.21 ⁻² | 1.37 ⁻² | |
| 1-131 | 9.39 ⁻² | 0.97 | 1.11 ⁻¹ | 8.98 ⁻² | 1.03 ⁻¹ | |
| 2-6 | 2.51 ⁻¹ | 1.20 | 2.55 ⁻¹ | 2.52 ⁻¹ | 2.48 ⁻¹ | 2.52 ⁻¹ |
| 2-7 | 2.53 ⁻¹ | 1.05 | 2.60 ⁻¹ | 2.57 ⁻¹ | 2.54 ⁻¹ | 2.60 ⁻¹ |
| 2-8 | 8.07 ⁻¹ | 0.99 | 8.23 ⁻¹ | 8.06 ⁻¹ | 8.02 ⁻¹ | 8.12 ⁻¹ |
| 2-9 | 1.89 ⁻² | 0.98 | 1.92 ⁻² | 1.93 ⁻² | 1.91 ⁻² | |
| 2-40 | 2.36 ⁻¹ | 0.97 | 2.34 ⁻¹ | 2.35 ⁻¹ | 2.45 ⁻¹ | |
| 2-43 | 1.88 ⁻¹ | 0.97 | 1.90 ⁻¹ | 1.91 ⁻¹ | 2.00 ⁻¹ | |
| 2-44 | 5.69 ⁻¹ | 0.97 | 5.55 ⁻¹ | 5.62 ⁻¹ | 5.87 ⁻¹ | |
| 2-46 | 2.00 ⁻¹ | 1.01 | 1.92 ⁻¹ | 1.94 ⁻¹ | 2.00 ⁻¹ | |
| 3-6 | 1.10 ⁻² | 1.24 | 1.10 ⁻² | 1.11 ⁻² | 1.11 ⁻² | |
| 3-7 | 2.84 ⁻¹ | 1.13 | 2.85 ⁻¹ | 2.79 ⁻¹ | 2.78 ⁻¹ | 2.84 ⁻¹ |
| 3-9 | 3.19 ⁻¹ | 1.07 | 3.25 ⁻¹ | 3.19 ⁻¹ | 3.17 ⁻¹ | 3.22 ⁻¹ |
| 3-10 | 2.73 ⁻¹ | 0.96 | 2.83 ⁻¹ | 2.77 ⁻¹ | 2.75 ⁻¹ | 2.81 ⁻¹ |
| 3-11 | 9.96 ⁻² | 0.89 | 1.02 ⁻¹ | 1.03 ⁻¹ | 9.94 ⁻² | 1.02 ⁻¹ |
| 3-12 | 1.53 ⁻³ | 1.21 | 1.38 ⁻³ | 1.36 ⁻³ | 1.32 ⁻³ | |
| 3-14 | 4.15 ⁻³ | 0.61 | 4.53 ⁻³ | 4.61 ⁻³ | 4.76 ⁻³ | |
| 3-15 | 7.84 ⁻² | 0.72 | 8.05 ⁻² | 7.06 ⁻² | 8.00 ⁻² | 7.93 ⁻² |
| 3-28 | 9.23 ⁻² | 0.44 | 9.74 ⁻² | 1.01 ⁻¹ | 9.51 ⁻² | |
| 3-29 | 7.35 ⁻² | 0.34 | 7.72 ⁻² | 7.87 ⁻² | 7.17 ⁻² | |
| 3-43 | 2.33 ⁻¹ | 0.94 | 2.29 ⁻¹ | 2.29 ⁻¹ | 2.38 ⁻¹ | |
| 4-6 | 2.20 ⁻³ | 1.62 | 2.23 ⁻³ | 2.23 ⁻³ | 2.20 ⁻³ | |
| 4-12 | 1.30 ⁻¹ | 0.94 | 1.31 ⁻¹ | 1.32 ⁻¹ | 1.28 ⁻¹ | |
| 4-13 | 2.07 ⁻¹ | 0.83 | 2.12 ⁻¹ | 2.10 ⁻¹ | 2.07 ⁻¹ | |
| 4-28 | 6.41 ⁻² | 0.51 | 6.59 ⁻² | 6.76 ⁻² | 6.39 ⁻² | |
| 4-48 | 8.96 ⁻² | 0.96 | 8.88 ⁻² | 8.86 ⁻² | 9.33 ⁻² | |
| 4-49 | 1.49 ⁻¹ | 1.03 | 1.46 ⁻¹ | 1.48 ⁻¹ | 1.54 ⁻¹ | |
| 5-6 | 6.25 ⁻³ | 2.17 | 2.83 ⁻³ | 2.87 ⁻³ | 2.78 ⁻³ | |
| 5-10 | 6.54 ⁻³ | 1.48 | 4.67 ⁻³ | 4.73 ⁻³ | 4.76 ⁻³ | |
| 5-11 | 3.39 ⁻² | 1.11 | 3.10 ⁻² | 2.98 ⁻² | 3.00 ⁻² | |
| 5-12 | 2.14 ⁻¹ | 1.15 | 1.89 ⁻¹ | 1.87 ⁻¹ | 1.83 ⁻¹ | |
| 5-14 | 5.82 ⁻¹ | 1.00 | 5.93 ⁻¹ | 5.85 ⁻¹ | 5.78 ⁻¹ | 5.89 ⁻¹ |
| 5-15 | 1.05 ⁻¹ | 0.82 | 1.34 ⁻¹ | 1.19 ⁻¹ | 1.33 ⁻¹ | 1.33 ⁻¹ |
| 5-28 | 5.47 ⁻² | 0.53 | 1.05 ⁻¹ | 1.07 ⁻¹ | 1.01 ⁻¹ | |
| 5-29 | 2.33 ⁻² | 0.42 | 5.73 ⁻² | 5.96 ⁻² | 5.38 ⁻² | |
| 5-47 | 3.64 ⁻³ | 0.91 | 5.11 ⁻³ | 4.45 ⁻³ | 5.75 ⁻³ | |
| 5-49 | 7.80 ⁻² | 0.98 | 7.92 ⁻² | 7.76 ⁻² | 8.18 ⁻² | |

Notes. Index number corresponds to that in Table 8.^(a) GRASP data from the work of Aggarwal et al. (2004). ^(b) Data in CHIANTI are from the work of Landi & Gu (2006). ^(c) The SUPERSTRUCTURE (SS) calculations are from the work of Chen et al. (2003). ^(d) x^y denotes $x \times 10^y$.

resonance region, comparable to our present ICFT *R*-matrix calculation). Good agreement is obtained between the present results and those of Loch et al. for the background cross-section (e.g. $\sim 10\%$ at an electron energy of 1100 eV). The cross-section

convoluted by a Gaussian profile (a width of 30 eV, comparable with resolution of present detectors in the laboratory) also shows agreement except for that around energies of 870 eV. At energies of 910 eV and 964 eV, the present ICFT *R*-matrix results show a better agreement (6% and 19%) with laboratory measurement (Brown et al. 2006) than results of Chen (2007, 24% and 28%) and Loch et al. (2006, 26% and 33%). This results in a slightly lower Υ than previous results, see Fig. 4-b. An isolated resonance approximation has been employed by Landi & Gu (2006) to take the resonances in electron-impact excitation into account. However, their Υ at lower temperatures ($T_e \leq 2 \times 10^6$ K) is far above that from the present calculation, by up to 30% around $T_e = 2.9 \times 10^5$ K. At higher temperatures, their results show good agreement with Chen's and Loch et al.'s data, as well as the present ICFT *R*-matrix calculations (to within 10%). Landi & Gu (2006) data is currently used by the astrophysical modelling code-CHIANTI v6. Over the entire temperature range, the Dirac *R*-matrix calculation of Loch et al. (2006) is slightly higher than the present ICFT *R*-matrix calculation, by about 7%, which is consistent with the difference level of atomic structure, e.g. the gf -value discussed above in Sect. 2.2.

For the stronger 3C excitation (1-27), see Fig. 5, the present ICFT *R*-matrix results agree well (better than 5%) with those from the DARC calculation performed by Loch et al. (2006) at the energies of 910 and 964 eV. Both are higher than the measurement (Brown et al. 2006) by $\sim 35\%$. For the DARC calculation of Chen (2007), the difference drops to about 20% when compared with experimental data. This mirrors the reduction in his reported *A*-values, and the weighted oscillator strengths shown above, due to the inclusion of target pseudo-states – a similar effect was noted by Fournier & Hansen (2005). The present result is also in agreement (8%) with that reported by Aggarwal et al. (2003), see the point at $E_e = 1020$ eV. The resulting effective collision strengths also show good agreement (about 7%) between the present results and the BPRM of Chen et al. (2003) and DARC of Loch et al. (2006) over temperatures of equilibrium abundance for Fe^{16+} . With decreasing electron temperature, the difference between the present results and the DW plus isolated resonance results of Landi & Gu (2006) increases, but is still less than 20% at $T_e = 2.9 \times 10^5$ K. The DARC results of Chen (2007) are slightly lower than the present ones, by about 10%.

A complete set of data for Fe^{16+} for the work of Loch et al. (2006) is available from the Oak Ridge National Laboratory (ORNL) Controlled Fusion Atomic Data Center (CFADC)⁷ and for Landi & Gu (2006) from CHIANTI v6. Thus, we make an extensive comparison (all excitation data from ground state $2s^2 2p^6 \ ^1S_0$) with them at low (3.0×10^5 K), intermediate (4.0×10^6 K) and high (1.0×10^7 K) temperatures, see Fig. 6. In this comparison, we take configuration, total angular momentum *J* and energy ordering as the “good” quantum numbers, following the work of Liang et al. (2009b) for the Na-like iso-electronic sequence. At the low temperature, 61% and 92% of transitions (circles in top panel of Fig. 6) show agreement of 20% and a factor of 2, respectively. And there is a trend that more weaker excitations show larger differences. However, the comparison with results from the isolated resonant approximation reveals that only 25% and 64% of transitions show agreement of 20% and a factor of 2, respectively. Most excitation data (87%) of Landi & Gu (2006) is lower than the present ICFT *R*-matrix calculations. As explained in our assessment of atomic structure, the difference in structure can not explain this large discrepancy. This suggests that the systematic lower values for Υ may be

⁷ <http://www-cfadc.phy.ornl.gov/>

Table 10. The level energies (Ryd) of Ni¹⁸⁺ from different calculations along with the compilation of NIST v3.

| ID | Level specification | NIST ^a | AS | FAC | GRASP ^b | CHIANTI ^c |
|----|--|-------------------|---------|---------|--------------------|----------------------|
| 1 | 2s ² 2p ⁶ 1S ₀ | | 0.00000 | | 0.0000 | |
| 2 | 2s ² 2p ⁵ 3s 3P ₂ | 64.7479 | 64.7742 | 64.6221 | 64.6011 | 64.7263 |
| 3 | 2s ² 2p ⁵ 3s 1P ₁ | 64.9059 | 64.9287 | 64.7897 | 64.7640 | 64.8740 |
| 4 | 2s ² 2p ⁵ 3s 3P ₀ | 66.0459 | 66.0775 | 65.9187 | 65.9039 | 66.0385 |
| 5 | 2s ² 2p ⁵ 3s 3P ₁ | 66.1407 | 66.1706 | 66.0193 | 66.0009 | 66.1251 |
| 6 | 2s ² 2p ⁵ 3p 3S ₁ | 67.2696 | 67.3214 | 67.1650 | 67.1257 | 67.3018 |
| 7 | 2s ² 2p ⁵ 3p 3D ₂ | 67.5241 | 67.5856 | 67.4291 | 67.3913 | 67.5202 |
| 8 | 2s ² 2p ⁵ 3p 3D ₃ | 67.7229 | 67.7786 | 67.6269 | 67.5876 | 67.7173 |
| 9 | 2s ² 2p ⁵ 3p 1P ₁ | 67.7987 | 67.8544 | 67.7073 | 67.6682 | 67.7830 |
| 10 | 2s ² 2p ⁵ 3p 3P ₂ | 67.9647 | 68.0153 | 67.8694 | 67.8324 | 67.9334 |
| 11 | 2s ² 2p ⁵ 3p 3P ₀ | 68.4879 | 68.5694 | 68.4048 | 68.3717 | 68.4646 |
| 12 | 2s ² 2p ⁵ 3p 3D ₁ | 68.7711 | 68.8455 | 68.6775 | 68.6441 | 68.7870 |
| 13 | 2s ² 2p ⁵ 3p 3P ₁ | 69.1003 | 69.1570 | 69.0003 | 68.9678 | 69.0941 |
| 14 | 2s ² 2p ⁵ 3p 1D ₂ | 69.1402 | 69.2008 | 69.0411 | 69.0097 | 69.1369 |
| 15 | 2s ² 2p ⁵ 3p 1S ₀ | 70.0837 | 70.2499 | 70.1372 | 70.1203 | 70.0599 |
| 16 | 2s ² 2p ⁵ 3d 3P ₀ | 71.0603 | 71.1264 | 70.9484 | 70.9199 | 71.0761 |
| 17 | 2s ² 2p ⁵ 3d 3P ₁ | 71.1490 | 71.2239 | 71.0377 | 71.0093 | 71.1644 |
| 18 | 2s ² 2p ⁵ 3d 3P ₂ | 71.3137 | 71.4019 | 71.2055 | 71.1776 | 71.3240 |
| 19 | 2s ² 2p ⁵ 3d 3F ₄ | 71.3092 | 71.4096 | 71.2029 | 71.1752 | 71.3248 |
| 20 | 2s ² 2p ⁵ 3d 3F ₃ | 71.3607 | 71.4437 | 71.2575 | 71.2340 | 71.3676 |
| 21 | 2s ² 2p ⁵ 3d 1D ₂ | 71.5080 | 71.5928 | 71.4098 | 71.3861 | 71.4998 |
| 22 | 2s ² 2p ⁵ 3d 3D ₃ | 71.6041 | 71.7083 | 71.5079 | 71.4847 | 71.5973 |
| 23 | 2s ² 2p ⁵ 3d 3D ₁ | 72.0028 | 72.1387 | 71.9452 | 71.9256 | 72.0192 |
| 24 | 2s ² 2p ⁵ 3d 3F ₂ | 72.6505 | 72.7348 | 72.5485 | 72.5263 | 72.6617 |
| 25 | 2s ² 2p ⁵ 3d 3D ₂ | 72.7265 | 72.8272 | 72.6191 | 72.6005 | 72.7346 |
| 26 | 2s ² 2p ⁵ 3d 1F ₃ | 72.7796 | 72.8836 | 72.6726 | 72.6564 | 72.7920 |
| 27 | 2s ² 2p ⁵ 3d 1P ₁ | 73.2823 | 73.4547 | 73.2548 | 73.2464 | 73.3387 |
| 28 | 2s2p ⁶ 3s 3S ₁ | 76.1637 | 76.0905 | 75.9685 | 75.9179 | 76.0394 |
| 29 | 2s2p ⁶ 3s 1S ₀ | 76.6922 | 76.6420 | 76.5136 | 76.4612 | 76.5453 |
| 30 | 2s2p ⁶ 3p 3P ₀ | | 78.8035 | 78.6856 | 78.6288 | 78.7562 |
| 31 | 2s2p ⁶ 3p 3P ₁ | 78.5640 | 78.8478 | 78.7275 | 78.6701 | 78.7972 |
| 32 | 2s2p ⁶ 3p 3P ₂ | | 79.1025 | 78.9785 | 78.9231 | 79.0459 |
| 33 | 2s2p ⁶ 3p 1P ₁ | 78.9731 | 79.2543 | 79.1374 | 79.0767 | 79.1836 |
| 34 | 2s2p ⁶ 3d 3D ₁ | | 82.5614 | 82.4049 | 82.3630 | 82.5247 |
| 35 | 2s2p ⁶ 3d 3D ₂ | | 82.5888 | 82.4203 | 82.3787 | 82.5451 |
| 36 | 2s2p ⁶ 3d 3D ₃ | | 82.6376 | 82.4501 | 82.4089 | 82.5807 |
| 37 | 2s2p ⁶ 3d 1D ₂ | | 83.0283 | 82.8611 | 82.8349 | 82.9545 |
| 38 | 2s ² 2p ⁵ 4s 3P ₂ | | 87.4340 | 87.2557 | 87.1882 | 87.3495 |
| 39 | 2s ² 2p ⁵ 4s 1P ₁ | 87.3449 | 87.4794 | 87.3103 | 87.2418 | 87.3995 |
| 40 | 2s ² 2p ⁵ 4p 3S ₁ | | 88.4761 | 88.3083 | 88.2410 | 88.4117 |
| 41 | 2s ² 2p ⁵ 4p 3D ₂ | | 88.5396 | 88.3755 | 88.3064 | 88.4710 |
| 42 | 2s ² 2p ⁵ 4p 3D ₃ | | 88.6148 | 88.4565 | 88.3882 | 88.5530 |
| 43 | 2s ² 2p ⁵ 4p 1P ₁ | | 88.6414 | 88.4864 | 88.4172 | 88.5784 |
| 44 | 2s ² 2p ⁵ 4p 3P ₂ | | 88.6935 | 88.5414 | 88.4719 | 88.6285 |
| 45 | 2s ² 2p ⁵ 4s 3P ₀ | | 88.7381 | 88.5592 | 88.4959 | 88.6644 |
| 46 | 2s ² 2p ⁵ 4s 3P ₁ | 88.6207 | 88.7610 | 88.5863 | 88.5223 | 88.6908 |
| 47 | 2s ² 2p ⁵ 4p 3P ₀ | | 89.0180 | 88.8778 | 88.8116 | 88.9147 |
| 48 | 2s ² 2p ⁵ 4p 3D ₁ | | 89.8241 | 89.6556 | 89.5915 | 89.7666 |
| 49 | 2s ² 2p ⁵ 4d 3P ₀ | | 89.8633 | 89.6923 | 89.6308 | 89.8053 |
| 50 | 2s ² 2p ⁵ 4d 3P ₁ | 89.7142 | 89.9037 | 89.7307 | 89.6695 | 89.8418 |
| 51 | 2s ² 2p ⁵ 4p 3P ₁ | | 89.9367 | 89.7797 | 89.7152 | 89.8858 |
| 52 | 2s ² 2p ⁵ 4p 1D ₂ | | 89.9566 | 89.7997 | 89.7347 | 89.9049 |
| 53 | 2s ² 2p ⁵ 4d 3F ₄ | 89.8783 | 89.9595 | 89.7800 | 89.7186 | 89.8919 |
| 54 | 2s ² 2p ⁵ 4d 3F ₃ | 89.8974 | 89.9696 | 89.7988 | 89.7381 | 89.9055 |
| 55 | 2s ² 2p ⁵ 4d 3P ₂ | | 89.9698 | 89.7945 | 89.7335 | 89.9028 |
| 56 | 2s ² 2p ⁵ 4d 1D ₂ | | 90.0223 | 89.8526 | 89.7923 | 89.9538 |
| 57 | 2s ² 2p ⁵ 4d 3D ₃ | | 90.0641 | 89.8883 | 89.8282 | 89.9894 |
| 58 | 2s ² 2p ⁵ 4p 1S ₀ | | 90.1459 | 90.0186 | 89.9571 | 90.0498 |
| 59 | 2s ² 2p ⁵ 4d 1P ₁ | 90.1334 | 90.2812 | 90.1093 | 90.0559 | 90.1881 |
| 60 | 2s ² 2p ⁵ 4f 3D ₁ | | 90.6112 | 90.4620 | 90.3808 | 90.5167 |

Notes. ^a Sources of the NIST v3 are from the work of [Sugar & Corliss \(1985\)](#) and references therein. ^b GRASP data are from the work of [Aggarwal & Keenan \(2006\)](#). ^c Data in CHIANTI are from the work of [Zhang et al. \(1987\)](#).

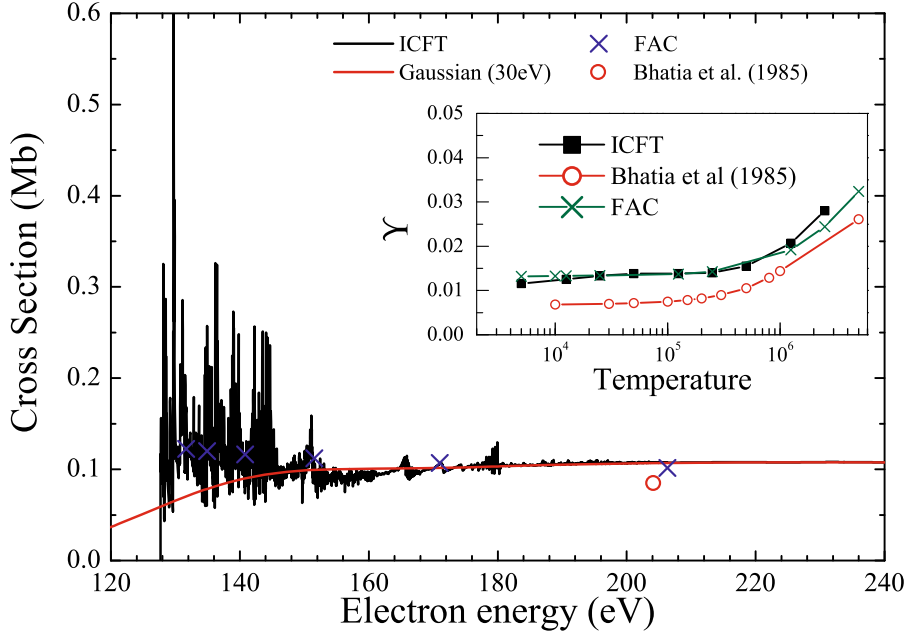


Fig. 2. Comparison of the collision cross-section and Υ of Si^{4+} for $2s^22p^6\ ^1S_0 \rightarrow 2s^22p^53d\ ^3D_1$ ($3D$) excitation between the present ICFT *R*-matrix and previous calculations. Red smooth solid line is Gaussian convolution with width of 30 eV. [Colour online]

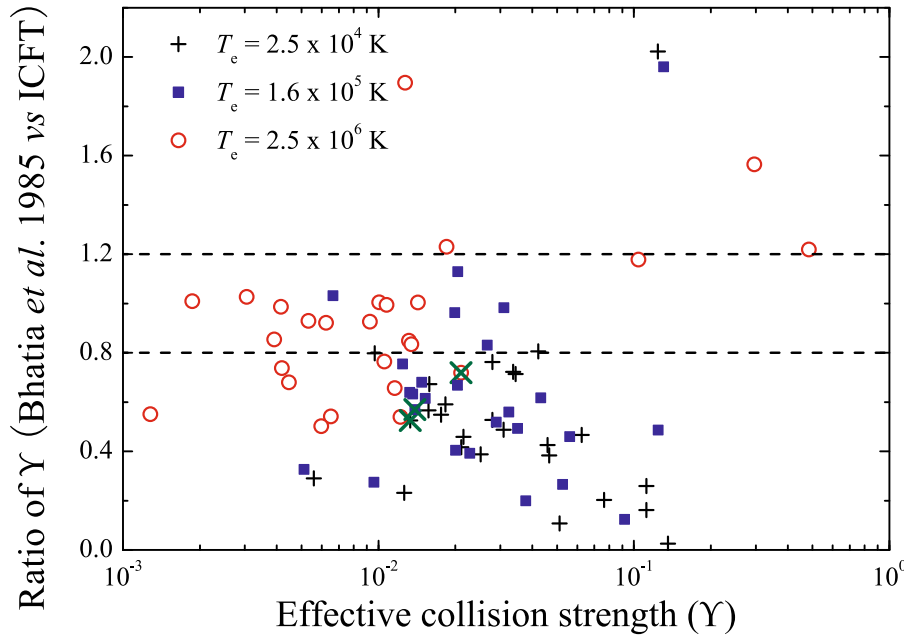


Fig. 3. An extensive comparison (all available excitations from the ground state) of effective collision strength Υ for Si^{4+} between the present ICFT *R*-matrix and previous available data (DW calculation of Bhatia et al. (1985), from CHIANTI v6.0 database) at low (2.5×10^4 K), intermediate (1.6×10^5 K, that of peak fraction in ionization equilibrium) and high (2.5×10^6 K) temperatures. Horizontal dashed lines denote agreement of 20%. “x” symbols correspond to the $3D$ transition in Fig. 2. [Colour online]

due to the limited number of resonances included in their isolated resonant approximation, viz., autoionizing levels from the following configurations: $2s^22p^6n_2l_2$, $2s^22p^53ln_3l_3$, $2s^22p^64ln_4l_4$ with $n_{2,3} \leq 45$, $n_4 \leq 10$, $l_2 \leq 9$, $l_3 \leq 7$, and $l_4 \leq 4$ included, see Landi & Gu (2006). At the high temperature, 91% of transitions are within 20% in the comparison between the ICFT and Dirac *R*-matrix calculations. The comparison with data of Landi & Gu (2006) shows that the percentage is up to 60%—a value comparable to the structure assessment. At the intermediate temperature of 4.0×10^6 K with peak fractional abundance in ionization equilibrium (Mazzotta et al. 1998; Bryans et al. 2006), the percentage is 55% and 88% when compared with data of Landi & Gu (2006) and Loch et al. (2006), respectively. This is within the range defined by the above mentioned extreme cases (low and high temperatures), being close to the case of the high

temperature. In other words, the resonance enhancement on the Υ has significantly decreased at the temperature of the peak fractional abundance in the ionization equilibrium. The differences at lower temperatures suggests that caution should be exercised when using data from the isolated resonance approximation for high-precision spectroscopic modelling of astrophysical and laboratory plasmas.

— Kr^{26+} Griffin et al. (2008) performed a 139-level *R*-matrix calculations using the Dirac method. Two separate calculations were done: one with radiation damping and one without. Figure 7 shows the cross-section (original and a Gaussian convolution with a width of 30 eV) and a comparison of Υ between our present ICFT *R*-matrix result and that of Griffin et al. (2008). Our original and convoluted cross-section show good agreement with data of Griffin et al. (2008), see Fig. 2-c in their work. The

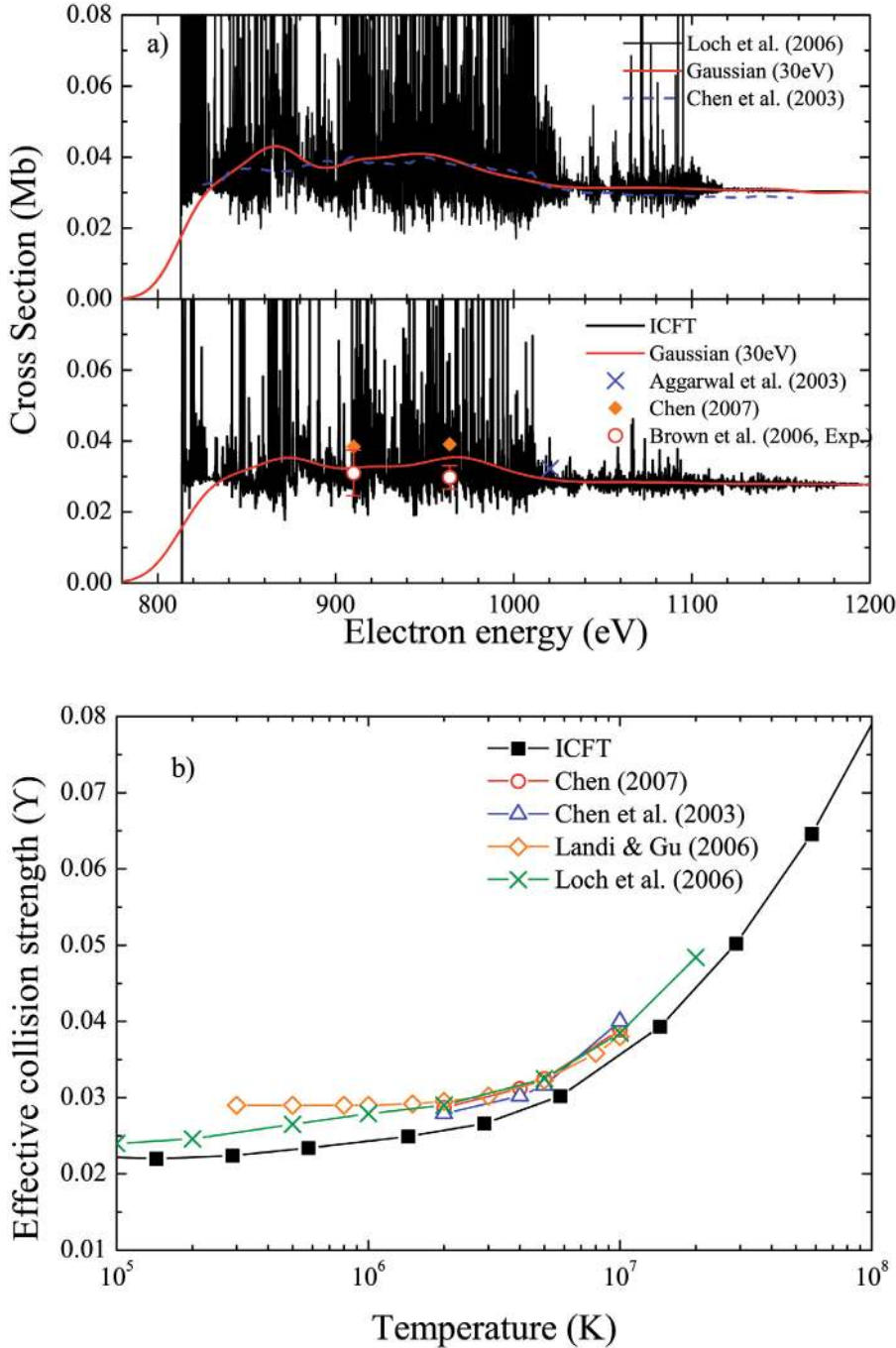


Fig. 4. Comparison of the collision cross-section and Υ of Fe^{16+} for $2s^22p^6\ ^1S_0 \rightarrow 2s^22p^53d\ ^3D_1$ ($3D$) excitation between the present ICFT R -matrix and previous calculations. **a)** *Top*: the result of [Loch et al. \(2006\)](#) who used a finer energy mesh (around 10 times) than present calculation. The smooth-lines are cross-sections convoluted by Gaussian with a width of 30 eV (solid: [Loch et al. 2006](#); dashed: [Chen et al. 2003](#)). *Bottom*: the present ICFT R -matrix result along with Gaussian convolution (the width of 30 eV) and previous Dirac R -matrix calculations ([Chen 2007](#), Gaussian convolution; [Aggarwal et al. 2003](#), unconvoluted), as well as experimental measurements of [Brown et al. \(2006\)](#) at two energies. **b)** The effective collision strength Υ from different R -matrix calculations, and the DW plus isolated resonance approximation employed by [Landi & Gu \(2006\)](#). [*Colour online*]

background agrees well with the DW calculation from [Bhatia et al. \(1985\)](#) – see the point at $E_e = 1904.8$ eV. The 27-level ($2s^22p^6$ and $2s^22p^53l$) BPRM calculation of [Gupta et al. \(2000\)](#) has no resonances above $E_e = 2000$ eV. Strong resonances attached to the $2s2p^63l$ and $2s^22p^54l$ configurations appear, as demonstrated in the work of [Griffin et al. \(2008\)](#). The cross-section at $E_e = 2040.9$ eV (derived by us from the collision strength given at $E_e = 150$ Ryd) of [Gupta et al. \(2000\)](#) agrees well with the background of present ICFT R -matrix calculation. The present resultant Υ is also consistent with the data of [Griffin et al. \(2008\)](#) both with and without radiative damping, being within 3% over the entire temperature range. Good agreement is also found when compared with Gupta et al.’s data.

Since a complete dataset of Υ of Dirac R -matrix data ([Griffin et al. 2008](#)) is available from the CFADC⁷, we make an extensive comparison of Υ between the two different R -matrix datasets for Kr^{26+} , as shown in Fig. 8. At the low temperature $T_e = 5.0 \times 10^6$ K, 75% of excitations from ground state show agreement of 20%. The percentage increases up to 88% at the high temperature of $T_e = 5.0 \times 10^7$ K.

[Griffin et al. \(2008\)](#) made a statistical analysis of Υ over temperatures from $T_e = 5.0 \times 10^6$ K to $T_e = 5.0 \times 10^7$ K for 9591 transitions among 139 levels, and found the average difference between the Υ with and without damping to be 1.58%. As we know, radiative rates have a dependence of q^4 (where q is residual charge) for $\delta n > 0$ transitions. In their Na-like iso-electronic

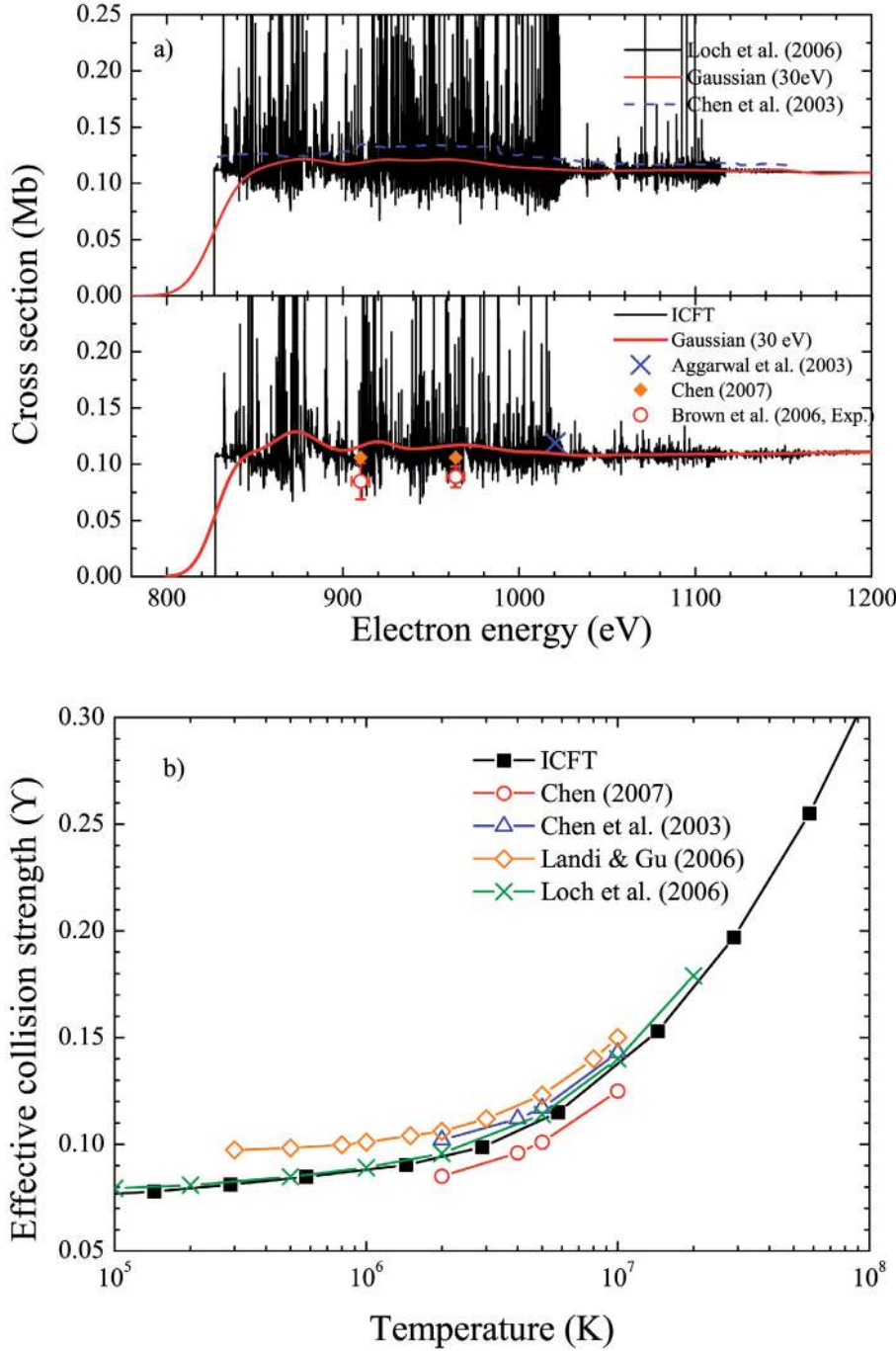


Fig. 5. Comparison of the collision cross-section and Υ of Fe^{16+} for $2s^2 2p^6 \ ^1S_0 \rightarrow 2s^2 2p^5 3d \ ^1P_1$ (3C) excitation between the present ICFT *R*-matrix and previous calculations. The same figure caption as in Fig. 4. [Colour online]

sequence *R*-matrix calculation, Liang et al. (2009b) tested that the radiative damping becomes dominant with increasing of ionic charge. So, the radiative damping effect for the present ions of the Ne-like iso-electronic sequence will be negligible. The present ICFT *R*-matrix calculations without radiative damping are accurate over the sequence in this respect.

From the above comparison for the three specified ions (Si^{4+} , Fe^{16+} and Kr^{26+}) spanning the sequence, we believe that the present ICFT *R*-matrix results (σ and Υ) have the comparable level of accuracy with other *R*-matrix calculations, including both Dirac and Breit-Pauli *R*-matrix methods. Except for Fe, Ni and Kr, the present results are the only *R*-matrix ones, to-date. For ions near neutral (below Si^{4+}), *R*-matrix with pseudostates

calculations are likely needed to model ionization loss, but the present are the best data available, to-date.

4.2. Iso-electronic trends of Υ 's

As noted in the work of Witthoef et al. (2007), the level mixing effect for higher excited levels strongly affects the behaviour of the Υ along the sequence. Similar level-ordering cross was identified by Liang et al. (2009b) in *R*-matrix EIE calculation of Na-like iso-electronic sequence. Witthoef & Badnell (2008) and Liang et al. (2009b) noticed that taking configuration, total angular momentum *J* and energy ordering as good quantum number is a better choice for level matching in comparison between two different calculations and investigation of Υ

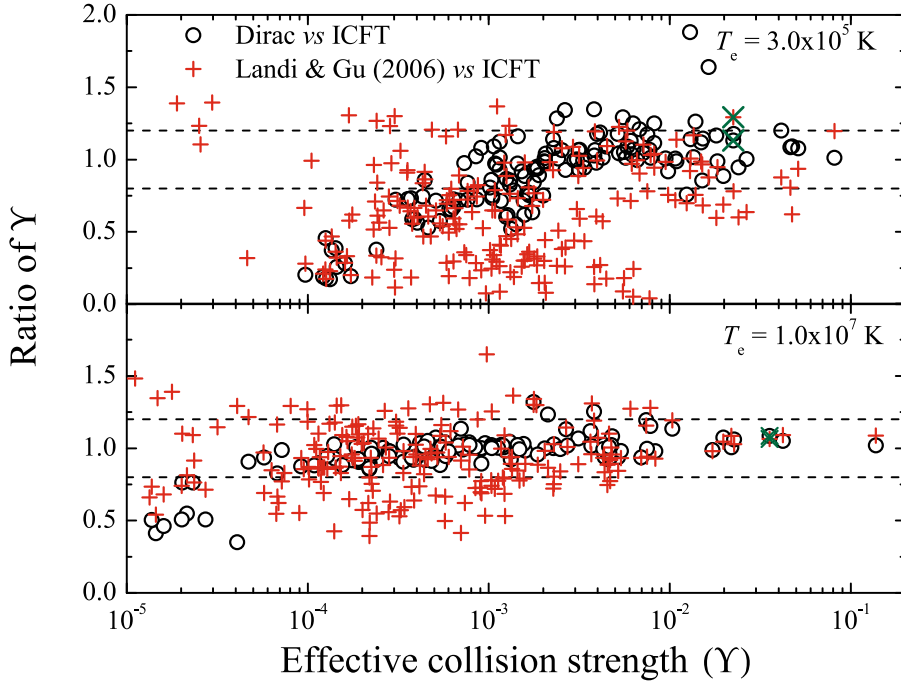


Fig. 6. An extensive comparison (all excitations from the ground state) of effective collision strength Υ of Fe^{16+} between the present ICFT R -matrix and Dirac R -matrix (Loch et al. 2006)⁷ calculations, as well as results of Landi & Gu (2006) using an isolated resonance approximation, at low (3.0×10^5 K) and high (1.0×10^7 K) temperatures. Horizontal dashed lines denote agreement of 20%. “x” symbols correspond to the 3D transition in Fig. 4. [Colour online]

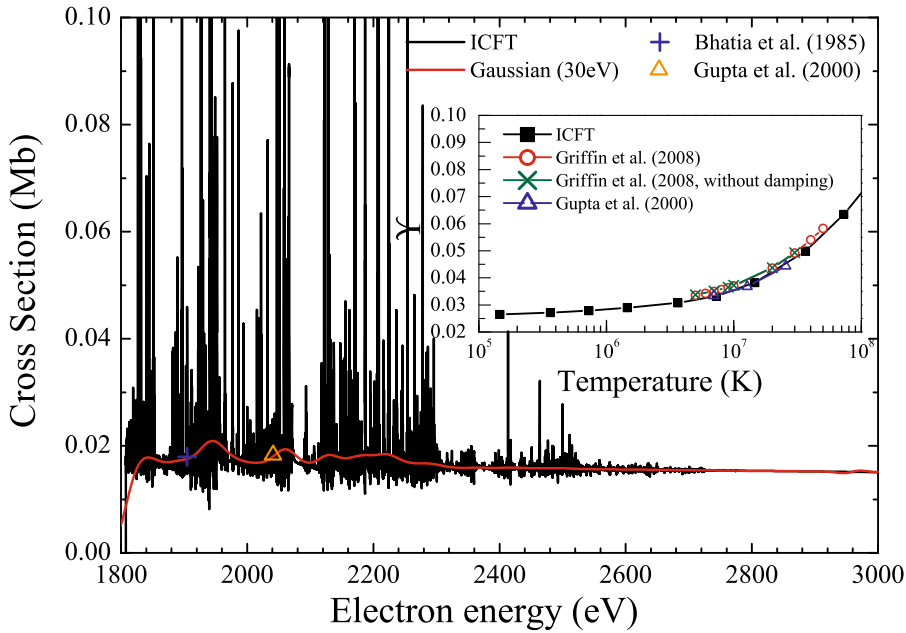


Fig. 7. Comparison of the collision cross-section and Υ of Kr^{26+} for $2s^2 2p^6 J = 0 \rightarrow 2s^2 2p^5 3d J = 1$ (3D) excitation between the present ICFT R -matrix and previous calculations including Dirac R -matrix results of Griffin et al. (2008) with and without radiative damping, Breit-Pauli R -matrix results of Gupta et al. (2000) and DW cross-sections of Bhatia et al. (1985) at $E_e = 1904.8$ eV. Red smooth solid line is Gaussian convolution with width of 30 eV. [Colour online]

along the iso-electronic sequence. We find this to be true again, and map all ions relative to the level ordering of Fe^{16+} in the following discussion, see Fig. 9. This satisfactorily eliminates uncertainty originating from the non-continuity of level-ordering along the sequence. The choice of reference ion, Fe here, is of course irrelevant.

In Fig. 10, we show effective collision strength Υ at $T_e = 10^3(q+1)^2$, $10^4(q+1)^2$ and $10^5(q+1)^2$ K along the sequence for four dominant and strong transition lines in Ne-like ions: $2s^2 2p^5 3s^3 P_1(3G), ^1P_1(3F) \rightarrow 2s^2 2p^6 ^1S_0$ (see Fig. 10a) and $2s^2 2p^5 3d^1 P_1(3C)$ and $^3D_1(3D) \rightarrow 2s^2 2p^6 ^1S_0$ (see Fig. 10b). At the low temperature of $10^3(q+1)^2$ K, spikes and/or dips are observed along the sequence for the $3s \rightarrow 2p$ transitions. However,

there are no clear spikes and/or dips for $3d \rightarrow 2p$ transitions. As pointed out by Withoef et al. (2007), such spikes/dips along the iso-electronic sequence at low temperature are due to the steady shifting of groups of resonances. This indirectly indicates that resonances are more important for the $3s \rightarrow 2p$ transitions than for the $3d \rightarrow 2p$ transitions. With increasing temperature, the spikes and/or dips disappear, as expected, because the resonance contribution becomes weaker and eventually negligible. For the 3D transition line, the Υ increases again below $Z = 15$ at the high temperature of $10^5(q+1)^2$ K. This is due to the high-energy collision strengths that are proportional to $gf/\Delta E$, as discussed for Si^{4+} for this transition line.

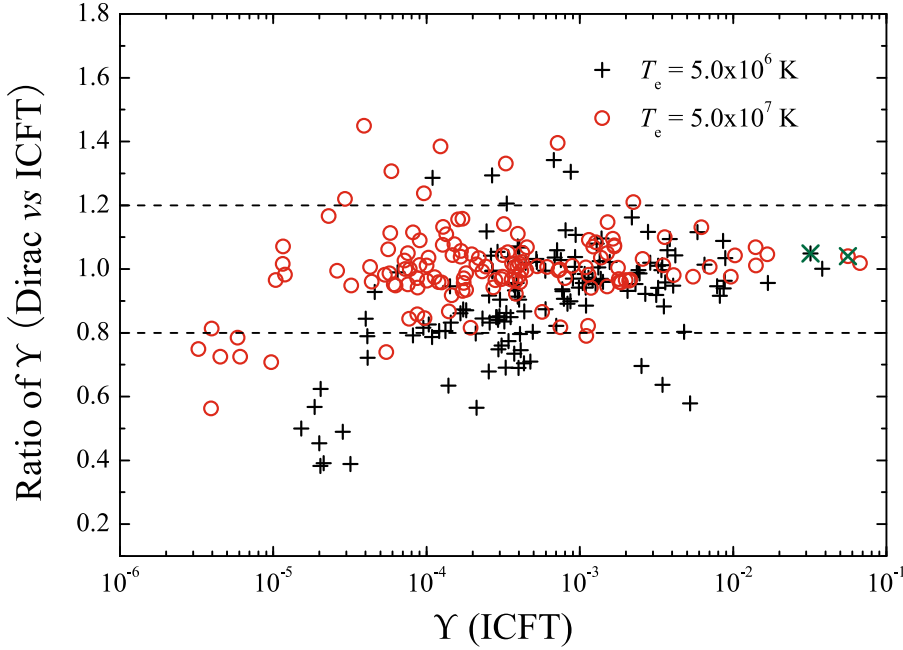


Fig. 8. An extensive comparison (all excitations from the ground state) of effective collision strength Υ for Kr^{26+} between the present ICFT *R*-matrix and Dirac *R*-matrix (Griffin et al. 2008)⁷ calculations at low (5.0×10^6 K) and high (5.0×10^7 K) temperatures. Horizontal dashed lines denote agreement of 20%. “ \times ” symbols correspond to the $3D$ transition in Fig. 7. [Colour online]

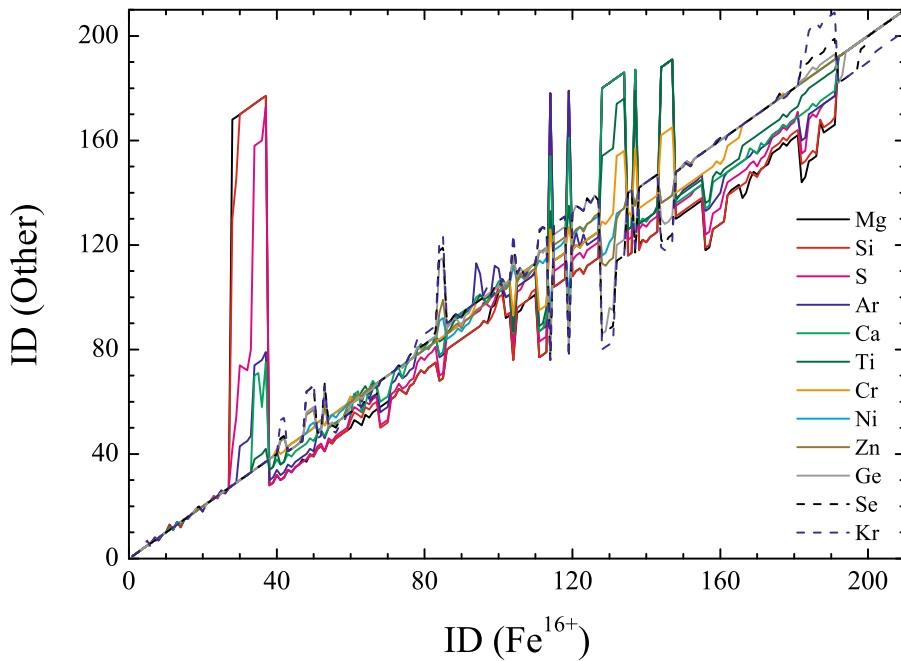


Fig. 9. The level ordering with the original level index (ID) relative to the ordering of Fe^{16+} by mapping according to the good quantum number – configuration, total angular momentum J and energy ordering for ions spanning the entire sequence. The spikes and dips are due to the shift of a given level, for example, $2s2p^63l$ (28–37) levels in Fe^{16+} move to levels above 120 in Si^{4+} . [Colour online]

5. Summary

We have performed 209-level ICFT *R*-matrix calculations of electron impact excitations with extensive configuration interaction (1337 LS terms or 2775 fine-structure levels) for all ions of the Ne-like iso-electronic sequence from Na^+ to Kr^{26+} . The present work is the most extensive and complete *R*-matrix data for modelling, to-date.

Good agreement with the available NIST v3 experimentally derived or CHIANTI v6 observed data and the results of others for level energies and gf -values for six specific ions (Si^{4+} , Ar^{8+} , Ca^{10+} , Fe^{16+} , Ni^{18+} and Kr^{26+}) spanning the iso-electronic sequence supports the reliability of the present *R*-matrix excitation

data. This was confirmed specifically, by detailed comparisons of Ω/σ and Υ for Si^{4+} , Fe^{16+} and Kr^{26+} .

The comparison (in the cases of Fe^{16+} and Kr^{26+}) with calculations using fully relativistic Dirac *R*-matrix method reveals that present excitation data from ICFT *R*-matrix shows the same level of accuracy. Excellent agreement of atomic structure for lower charged ions, e.g. Si^{4+} , gives us insight that the present excitation data is better than previous data (from the DW approximation) extensively used by the astrophysical and spectroscopic communities. It is noted that the isolated resonance approach appears to underestimate the resonant enhancement of Υ for the majority of excitations in the case of Fe^{16+} .

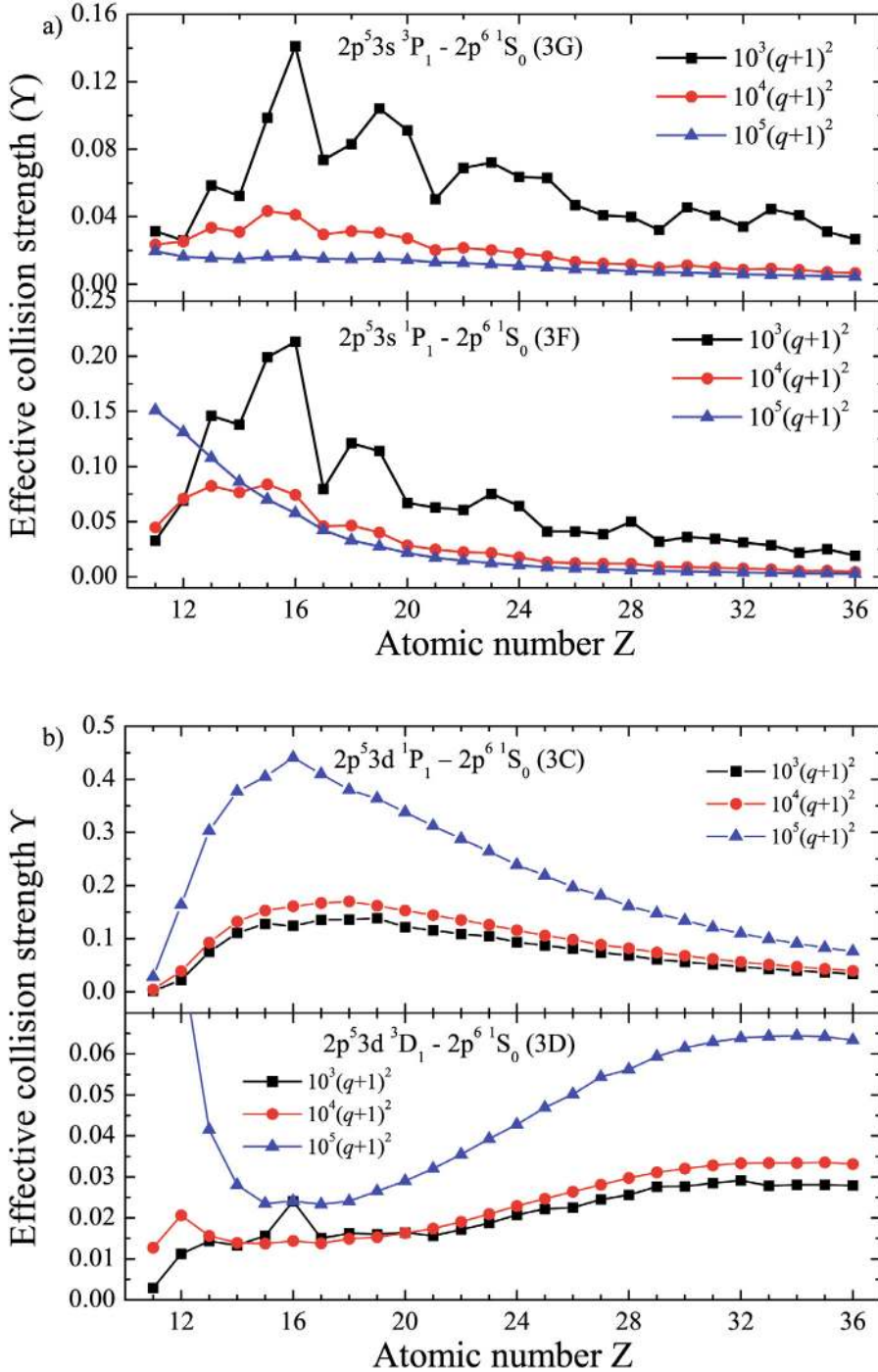


Fig. 10. Effective collision strength (Υ) at temperatures of $T_e = 10^{3,4,5}(q+1)^2$ K (here $q = Z - 10$) along the iso-electronic sequence. **a)** $2s^2 2p^5 3s \ ^3P_1(3G)$ and $^1P_1(3F) \rightarrow 2s^2 2p^6 \ ^1S_0$ transitions; **b)** $2s^2 2p^5 3d \ ^1P_1(3C)$ and $^3D_1(3D) \rightarrow 2s^2 2p^6 \ ^1S_0$ transitions. [Colour online]

By excluding the level crossing effects on the Υ , we examined the iso-electronic trends of the effective collision strengths. A complicated pattern of spikes and dips of Υ at low temperatures was noted again along the sequence, which precludes interpolation in Z . With increasing temperature, the difference between the present ICFT R -matrix and previous DW results decreases as expected.

The data are made available through archives of the APAP website [1](#) in the ADAS adf04 format (Summers 2004), OPEN-ADAS 3 and CHIANTI⁸.

⁸ <http://www.chianti.rl.ac.uk/>

In conclusion, we have generated an extensive set of reliable excitation data utilizing the ICFT R -matrix method for spectroscopy/diagnostic research within the astrophysical and fusion communities. This will replace data from DW and isolated resonance approaches presently used by these communities, for most ions, and its use can be expected to identify new lines and may overcome some shortcomings in present astrophysical modelling, as seen previously for Mg^{8+} (Del Zanna 2008), Fe^{6+} and Fe^{7+} (Del Zanna 2009a,b), and Si^{9+} (Liang et al. 2009c).

Table 13. Comparison of the weighted oscillator strength gf between the AS and other calculations for Kr^{26+} .

| $i - j$ | AS | | MCDF ^a | RFG00 ^b | ZSC87 ^c |
|---------|--------------|-----------|-------------------|--------------------|--------------------|
| | gfl | gfv/gfl | | | |
| 1–3 | 1.34^{-1d} | 0.83 | 1.34^{-1} | | 1.34^{-1} |
| 1–7 | 7.86^{-2} | 0.96 | 8.45^{-2} | | 8.45^{-2} |
| 1–17 | 4.45^{-3} | 0.96 | 6.41^{-3} | 7.79^{-3} | 6.00^{-3} |
| 1–23 | 1.53^{+0} | 1.00 | 1.55^{+0} | 1.54^{+0} | 1.55^{+0} |
| 1–27 | 1.90^{+0} | 1.00 | 1.93^{+0} | 1.94^{+0} | 2.09^{+0} |
| 1–31 | 8.90^{-2} | 1.01 | 8.97^{-2} | 8.75^{-2} | 9.70^{-2} |
| 1–33 | 3.12^{-1} | 1.06 | 3.05^{-1} | 3.05^{-1} | 3.78^{-1} |
| 1–39 | 2.38^{-2} | 0.69 | 2.48^{-2} | 2.47^{-2} | 2.30^{-2} |
| 1–47 | 2.44^{-3} | 0.93 | 3.26^{-3} | | 3.90^{-2} |
| 1–54 | 6.88^{-2} | 0.95 | 7.94^{-2} | 6.80^{-2} | 5.00^{-3} |
| 1–55 | 4.20^{-1} | 0.97 | 4.29^{-1} | 4.34^{-2} | 4.12^{-1} |
| 1–71 | 3.15^{-1} | 0.99 | 3.38^{-1} | 3.30^{-1} | 3.11^{-1} |
| 1–79 | 2.19^{-2} | 0.69 | 2.97^{-2} | 3.33^{-2} | |
| 1–81 | 2.15^{-2} | 0.98 | 1.77^{-2} | 1.30^{-2} | |
| 1–83 | 1.17^{-1} | 0.96 | 1.20^{-1} | 1.17^{-1} | |
| 1–97 | 2.03^{-1} | 0.95 | 2.24^{-1} | 2.33^{-1} | |
| 1–123 | 1.58^{-3} | 0.91 | 2.50^{-3} | | |
| 1–131 | 1.11^{-1} | 0.99 | 1.31^{-1} | 1.37^{-1} | |

Notes. Index number corresponds to that in Table 12. ^(a) Corresponds to the work of Griffin et al. (2008). ^(b) RFG00 refers to the calculation of Rice et al. (2000). ^(c) ZSC87 refers to the calculation of Zhang et al. (1987). ^(d) x^y denotes $x \times 10^y$.

Table 14. The energy meshes (in unit of q^2 , residual charge of ion) used for each ion.

| mesh | Atomic number | | | | |
|--------------------|---------------|-------|-------|-------|-------|
| | q^2 Ryd | 11–14 | 15–17 | 18–30 | 31–36 |
| 1×10^{-4} | | • | | | |
| 5×10^{-5} | | | • | | |
| 1×10^{-5} | | | | • | |
| 5×10^{-6} | | | | | • |

Acknowledgements. The work of the UK APAP Network is funded by the UK STFC under grant no. PP/E001254/1 with the University of Strathclyde. G.Y.L. thanks H. E. Mason, G. Del Zanna, P. J. Storey and K. A. Berrington for some helpful discussions.

References

Aggarwal, K. M., Keenan, F. P., & Msezane, A. Z. 2003, ApJS, 144, 169
 Aggarwal, K. M., & Keenan, F. P. 2006, A&A, 460, 959
 Aggarwal, K. M., & Keenan, F. P. 2008, A&A, 488, 365
 Badnell, N. R. 1986, J. Phys. B: At. Mol. Opt. Phys., 19, 3827
 Badnell, N. R., & Griffin, D. C. 1999, J. Phys. B: At. Mol. Opt. Phys., 32, 2267
 Badnell, N. R., & Griffin, D. C. 2001, J. Phys. B: At. Mol. Opt. Phys., 34, 681
 Beiersdorfer, P., Behar, E., Boyce, K. R., et al. 2002, ApJ, 576, L169

Beiersdorfer, P., Goeler, S. V., Bitter, M., & Thorn, D. B. 2001, Phys. Rev. A, 64, 032705
 Berrington, K. A., Eissner, W., & Norrington, P. H. 1995, Comput. Phys. Commun., 92, 290
 Berrington, K. A., Ballance, C. P., Griffin, D. C., & Badnell, N. R. 2005, J. Phys. B: At. Mol. Opt. Phys., 38, 1667
 Bhatia, A. K., Feldman, U., & Seely, J. F. 1985, At. Data Nucl. Data Tables, 32, 435
 Brown, G. V., Beiersdorfer, P., Chen, H., et al. 2006, Phys. Rev. Lett., 96, 253201
 Bryans, P., Badnell, N. R., Gorczyca, T. W., et al. 2006, ApJ, 691, 1540
 Bryans, P., Landi, E., & Savin, D. W. 2009, ApJS, 167, 343
 Burgess, A. 1974, J. Phys. B: At. Mol. Opt. Phys., 7, L364
 Burgess, A., & Tully, J. A. 1991, A&A, 254, 436
 Chen, G. X. 2007, Phys. Rev. A, 76, 062708
 Chen, G. X. 2008, MNRAS, 386, L62
 Chen, G. X., Pradhan, A. K., & Eissner, W. 2003, J. Phys. B: At. Mol. Opt. Phys., 36, 453
 Chen, G. X., Kirby, K., Silver, E., et al. 2006, Phys. Rev. Lett., 97, 143201
 Del Zanna, G. 2009a, A&A, 508, 501
 Del Zanna, G. 2009b, A&A, 508, 513
 Del Zanna, G., & Ishikawa, Y. 2009, A&A, 508, 1517
 Del Zanna, G., Rozum, I., & Badnell, N. R. 2008, A&A, 487, 1203
 Dere, K. P., Landi, E., Young, P. R., et al. 2009, A&A, 498, 915
 Fournier, K. B., & Hansen, S. B. 2005, Phys. Rev. A, 71, 012717
 Griffin, D. C., Badnell, N. R., & Pindzola, M. S. 1998, J. Phys. B: At. Mol. Opt. Phys., 31, 3713
 Griffin, D. C., Ballance, C. P., Mitnik, D. M., & Berengut, J. C. 2008, J. Phys. B: At. Mol. Opt. Phys., 41, 215201
 Gu, M. F. 2008, Can. J. Phys., 86, 675
 Gu, M. F., Beiersdorfer, P., Brown, G. V., et al. 2004, ApJ, 607, L143
 Gupta, G. P., Deb, N. C., & Msezane, A. Z. 2000, Phys. Scr., 61, 175
 Hummer, D. G., Berrington, K. A., Eissner, W., et al. 1993, A&A, 279, 298
 Landi, E., & Gu, M. F. 2006, ApJ, 640, 1171
 Lepson, J. K., Beiersdorfer, P., Behar, E., & Kahn, S. M. 2003, ApJ, 590, 604
 Liang, G. Y., Whiteford, A. D., & Badnell, N. R. 2008, J. Phys. B: At. Mol. Opt. Phys., 41, 235203
 Liang, G. Y., Whiteford, A. D., & Badnell, N. R. 2009a, A&A, 500, 1263
 Liang, G. Y., Whiteford, A. D., & Badnell, N. R. 2009b, J. Phys. B: At. Mol. Opt. Phys., 42, 225002
 Liang, G. Y., Whiteford, A. D., & Badnell, N. R. 2009c, A&A, 499, 943
 Loch, S. D., Pindzola, M. S., Ballance, C. P., & Griffin, D. C. 2006, J. Phys. B: At. Mol. Opt. Phys., 39, 85
 Martin, W. C., & Zalubas, R. 1983, J. Phys. Chem. Ref. Data, 12, 323
 Mathews, D. L., Hagelstein, P. L., Rosen, M. D., et al. 1985, Phys. Rev. Lett., 54, 110
 Mazzotta, P., Mazzitelli, G., Colafrancesco, S., & Vittorio, N. 1998, A&AS, 133, 403
 Norrington, P. H., & Grant, I. P. 1987, J. Phys. B: At. Mol. Opt. Phys., 20, 4869
 Rice, J. E., Fournier, K. B., Goetz, J. A., Marmar, E. S., & Terry, J. L. 2000, J. Phys. B: At. Mol. Opt. Phys., 33, 5435
 Saloman, E. B. 2007, J. Phys. Chem. Ref. Data, 36, 215
 Shirai, T., Sugar, J., & Musgrove, A. 1999, unpublished, see <http://physics.nist.gov/PhysRefData/ASD/Html/ref.html#Kelly>
 Smith, B. W., Raymond, J. C., & Mann, J. B. 1985, ApJ, 298, 898
 Sugar, J., & Corliss, C. 1985, in Atomic Energy Levels of the Iron Period Elements Potassium Through Nickel, 14, Suppl. 2
 Summers, H. P. 2004, The ADAS User manual version 2.6
<http://www.adas.ac.uk/>
 Tomaselli, F. G., Rocca, J. J., Shlyaptshev, V. N., & Macchietto, C. D. 1997, Phys. Rev. A, 55, 1437
 Zhang, H. L., Sampson, D. H., Clark, R. E. H., & Mann, J. B. 1987, At. Data Nucl. Data Tables, 37, 17
 Witthoef, M. C., Whiteford, A. D., & Badnell, N. R. 2007, J. Phys. B: At. Mol. Opt. Phys., 40, 2969
 Witthoef, M. C., & Badnell, N. R. 2008, A&A, 481, 543